Determining the COB location along the Iberian margin and Galicia Bank from gravity anomaly inversion, residual depth anomaly and subsidence analysis.

L. Cowie, N. Kusznir, Gianreto Manatschal

Geophysical Journal International

Geophys. J. Int. (2015) **203,** 1355–1372
GJI Geodynamics and tectonics

doi: 10.1093/gji/ggv367

Determining the COB location along the Iberian margin and Galicia Bank from gravity anomaly inversion, residual depth anomaly and subsidence analysis

Leanne Cowie,[1] Nick Kusznir[1] and Gianreto Manatschal[2]

[1]*Earth, Ocean and Ecological Sciences, University of Liverpool, Liverpool, L69 3BX, United Kingdom. E-mail: leanne.cowie.87@gmail.com*
[2]*EOST-CGS (UMR 7517) CNRS, Université Louis Pasteur, 1 rue Blessig, F-67064 Strasbourg Cedex, France*

Accepted 2015 September 2. Received 2015 September 2; in original form 2014 October 17

SUMMARY

Knowledge and understanding of the ocean–continent transition (OCT) structure, continent–ocean boundary (COB) location and crustal type are of critical importance in evaluating rifted continental margin formation and evolution. OCT structure, COB location and magmatic type also have important implications for the understanding of the geodynamics of continental breakup and in the evaluation of petroleum systems in deep-water frontier oil and gas exploration at rifted continental margins. Mapping the distribution of thinned continental crust and lithosphere, its distal extent and the start of unequivocal oceanic crust and hence determining the OCT structure and COB location at rifted continental margins is therefore a generic global problem. In order to assist in the determination of the OCT structure and COB location, we present methodologies using gravity anomaly inversion, residual depth anomaly (RDA) analysis and subsidence analysis, which we apply to the west Iberian rifted continental margin. The west Iberian margin has one of the most complete data sets available for deep magma-poor rifted margins, so there is abundant data to which the results can be calibrated. Gravity anomaly inversion has been used to determine Moho depth, crustal basement thickness and continental lithosphere thinning; subsidence analysis has been used to determine the distribution of continental lithosphere thinning; and RDAs have been used to investigate the OCT bathymetric anomalies with respect to expected oceanic bathymetries at rifted continental margins. These quantitative analytical techniques have been applied to the west Iberian rifted continental margin along profiles IAM9, Lusigal 12 (with the TGS-extension) and ISE-01. Our predictions of OCT structure, COB location and magmatic type (i.e. the volume of magmatic addition, whether the margin is 'normal' magmatic, magma-starved or magma-rich) have been tested and validated using ODP wells (Legs 103, 149 and 173), which provide observational constraints on the west Iberian margin.

Key words: Gravity anomalies and Earth structure; Continental margins: divergent; Dynamics: gravity and tectonics.

1 INTRODUCTION

Knowledge of the structure of the ocean–continent transition (OCT), the location of the continent–ocean boundary (COB), magmatic type (i.e. the volume of magmatic addition, whether the margin is 'normal' magmatic, magma-poor or magma-rich) and the distribution of oceanic and continental lithosphere are key to understanding present day rifted continental margin architecture and evolution. Rifted continental margins can be categorized into three primary magmatic types: 'normal' magmatic and two end members: magma-poor and magma-rich. A 'normal' magmatic rifted continental margin has magmatic addition, which results in oceanic crust of approximately 7 km in thickness (White *et al.* 1992). Magma-poor rifted continental margins are often characterized by a wide OCT, extreme crustal thinning accompanied by normal faulting (Boillot *et al.* 1980; Manatschal 2004; Reston 2009) and anomalously small fractions of magmatism leading to mantle exhumation prior to oceanic spreading (Pérez-Gussinyé 2012). Magma-rich margins are characterized by thick wedges of volcanic flows (Hinz 1981), shown on seismic data as seaward dipping reflectors (SDRs), large amounts of syn-rift magmatic extrusives and intrusives (Coffin & Eldholm 1994), high velocity lower crust seaboard of the continental rifted margin (Franke 2013), and the crustal thinning may occur over a short distance. The determination of rifted

continental margin magmatic type and OCT structure, which show great diversity globally, are important for understanding the geodynamic, tectonic and magmatic processes involved in rifted continental margin formation and their evolution to the present day. Understanding structure and formation processes of rifted continental margins is important, not only because they are a key component of the plate tectonic Wilson cycle (Wilson 1966) but also for deep-water hydrocarbon exploration. In this paper, we present a set of integrated quantitative analysis techniques for assisting in the determination of OCT structure, COB location and crustal type at rifted continental margins, which have been applied and tested on the west Iberian rifted continental margin, where independent observations from ODP wells are available for ground-truthing.

Numerous studies (e.g. Whitmarsh & Miles 1995; Pickup *et al.* 1996; Chian *et al.* 1999; Contrucci *et al.* 2004; Hopper *et al.* 2004; D'Acremont *et al.* 2005; White *et al.* 2008; Reston 2009; Autin *et al.* 2010; Unternehr *et al.* 2010; Zalán *et al.* 2011) have used various approaches to determine OCT structure and COB location of rifted continental margins. Techniques that have been used include the analysis of seismic reflection and refraction data, gravity and magnetic anomalies, bathymetric breaks and well data. The aims of these studies have focussed on: (i) distinguishing whether the OCT at a rifted continental margin is narrow or wide; (ii) determining the location of the distal extent of continental crust and the presence of any isolated ribbons of thinned continental crust and (iii) determining the magmatic type of a rifted continental margin.

The west Iberian rifted continental margin has abundant observational data; including seismic reflection and refraction surveys, magnetic anomalies and ODP well data. As a consequence it is a good natural laboratory for studying rifted continental margin evolution and has been used to demonstrate and test the methodologies and techniques used in this paper to determine OCT structure, COB location and magmatic type. On the west Iberian rifted continental margin, there have been many studies, which have addressed these and other questions. The application of seismic reflection and refraction data (e.g. Pickup *et al.* 1996; Whitmarsh & Sawyer 1996; Dean *et al.* 2000) and also seismic tomography (e.g. Zelt *et al.* 2003) has focussed on the determination of the OCT structure and the identification of the inner and outer bounds of the OCT. Detailed seismic mapping and borehole data has also been applied in order to further constrain the crustal type (e.g. Péron-Pinvidic *et al.* 2007), whilst magnetic anomalies have been used to tentatively locate the COB (e.g. Bronner *et al.* 2011). The determination of the magmatic type of a margin has been further constrained using seismic reflection data, magnetic anomalies and ODP well data as discussed in Pickup *et al.* (1996).

In this study, we have applied an integrated quantitative analysis of gravity anomaly inversion, residual depth anomaly (RDA) and subsidence analysis to the west Iberian rifted continental margin. Gravity anomaly inversion, incorporating a lithosphere thermal gravity anomaly correction, has been used to determine crustal basement thickness, Moho depth and continental lithosphere thinning across the west Iberian rifted continental margin. Sediment corrected RDAs have been used to calculate departures from standard oceanic water depths, as predicted by Crosby *et al.* (2006) and Stein & Stein (1992), whilst subsidence analysis has been used to give the distribution of continental lithosphere thinning. These techniques have been interpreted individually and together to identify the distribution of oceanic and thinned continental crust in order to determine the structure of the OCT and locate the COB.

The west Iberian margin is the result of rifting and continental breakup between the North American and Iberian plates during the Late Triassic to Early Cretaceous (Manatschal *et al.* 2001; Russell & Whitmarsh 2003; Manatschal 2004; Péron-Pinvidic *et al.* 2007). The Iberian Abyssal Plain is part of the magma-poor west Iberian margin (Chian *et al.* 1999) and is considered to be a type example of a sediment-starved magma-poor rifted continental margin (Sutra & Manatschal 2012). The west Iberian margin is subdivided into three main sections: Galicia margin to the north, the Iberian Abyssal Plain in the middle and the Tagus Abyssal Plain to the south (Manatschal *et al.* 2001). This paper focuses on three key profiles (IAM9, Lusigal 12 and ISE-01) along the Iberian Abyssal Plain and the Galicia margin highlighted in Fig. 1(a). The west Iberian rifted continental margin is, at present, considered to be one of the best studied rifted continental margins world-wide due to the abundant observational data available in the form of deep sea drilling (ODP Legs 103, 149 and 173, Boillot *et al.* 1987; Sawyer *et al.* 1994; Whitmarsh &

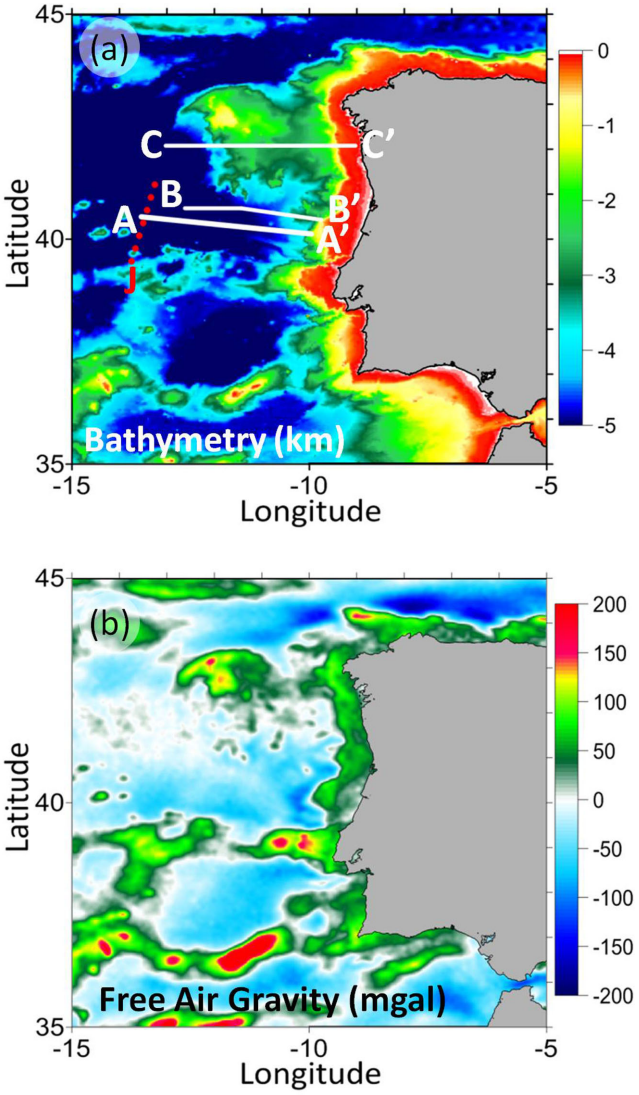

Figure 1. Data used in the gravity anomaly inversion, RDA and subsidence analysis for the Iberian Abyssal Plain and Galicia Bank. (a) Bathymetry (km; Amante & Eakins 2009). Locations of profiles IAM9 (A–A′), Lusigal 12 (with the TGS extension) (B–B′) and ISE-01 (C–C′) are indicated. The red dashed line indicates the location of the J anomaly (Dean *et al.* 2000; Whitmarsh *et al.* 2001; Bronner *et al.* 2011). (b) Free air gravity (mGal; Sandwell & Smith 2009).

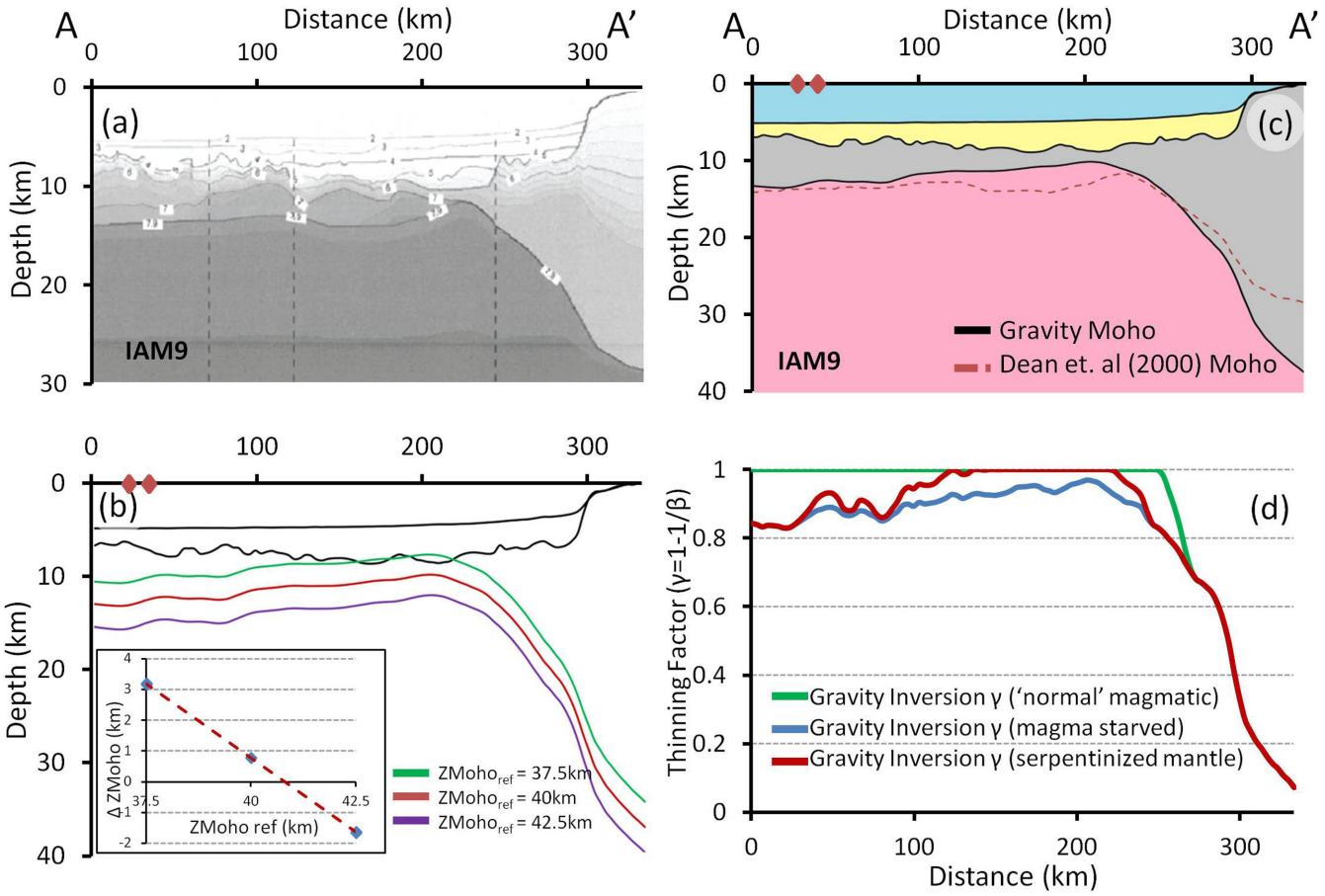

Figure 2. Gravity anomaly inversion results. (a) Cross-section from wide-angle seismic data for IAM9 (Dean *et al.* 2000) showing Moho depth. (b) Moho depths predicted from gravity anomaly inversion using reference Moho depths of 37.5, 40 and 42.5 km. Inset shows the calibration of reference Moho depth. Difference (Δ ZMoho) between gravity anomaly inversion predicted Moho and seismic Moho depth (Dean *et al.* 2000) plotted against reference Moho depth. Calibration of the reference Moho depth gives a reference Moho depth of 41 km. (c) Crustal cross section (A–A′) along profile IAM9 constructed using bathymetry (Amante & Eakins 2009), 2-D sediment thickness (Dean *et al.* 2000) and Moho depth from gravity anomaly inversion. The red dashed line shows the 7.9 km s^{-1} iso-velocity contour (Dean *et al.* 2000) representing the seismic Moho depth. The red diamonds indicate the location of the Moho depths, in the oceanic domain, used for calibration. (d) Continental lithosphere thinning factors (γ) predicted from gravity anomaly inversion with sensitivities to a 'normal' magmatic solution, a magma-starved solution and a solution for serpentinized mantle.

Sawyer 1996; Whitmarsh *et al.* 1998; Tucholke *et al.* 2007) combined with seismic reflection and refraction surveys (Manatschal *et al.* 2010).

Within the literature there are a range of different definitions of the OCT and COB (e.g. Whitmarsh & Miles 1995; Discovery 215 Working Group 1998; Dean *et al.* 2000; Manatschal *et al.* 2001; Péron-Pinvidic *et al.* 2007; Manatschal *et al.* 2010). Within this paper, however, we define the OCT as the region between unequivocal continental crust of 'normal' thickness and unequivocal oceanic crust; the lithosphere in this region is highly thinned, with complex tectonics, variable magmatism and possible mantle exhumation. We define the COB as the distal limit of unequivocal continental crust; however, determining the location of the COB is made difficult by the presence of exhumed mantle and complex tectonics. Another important term used is continental breakup age. Conceptually the term continental breakup may be used to either describe the point at which the continental crust ruptures and starts to separate, or when plate boundaries are localized by the onset of decompression melting and magmatic seafloor spreading. Within this paper, we use the latter definition (i.e. when plate boundaries are localized by the onset of decompression melting and magmatic seafloor spreading).

2 OCT STRUCTURE: PROFILE IAM9

Integrated quantitative analysis has been used to determine OCT structure, COB location and magmatic type along profile IAM9 (A–A′). Profile IAM9 has been used to describe the gravity anomaly inversion, RDA and subsidence analysis techniques in detail due to the availability of reliable seismic Moho depths (Dean *et al.* 2000), which are required for calibration of the reference Moho depth.

2.1 Crustal basement thickness and continental lithosphere thinning along IAM9 from gravity anomaly inversion

Gravity anomaly inversion has been used to determine crustal basement thickness, Moho depth and continental lithosphere thinning, which in turn give the distribution of oceanic and continental lithosphere. The data used within the gravity anomaly inversion are bathymetry (Amante & Eakins 2009; Fig. 1a), satellite derived free air gravity (Sandwell & Smith 2009; Fig. 1b), 2-D sediment thickness from wide angle seismic data (Dean *et al.* 2000; Fig. 2a) and ocean age isochrons from Müller *et al.* (1997).

The gravity anomaly inversion method is carried out in the 3-D spectral domain, using the scheme of Parker (1972) to predict Moho depth and hence determine crustal basement thickness. As the gravity anomaly inversion has been applied to rifted continental margin lithosphere, a lithosphere thermal gravity anomaly correction is incorporated to account for the elevated geothermal gradient within oceanic and rifted continental margin lithosphere. Failure to include the correction for the lithosphere thermal gravity anomaly can lead to predictions of Moho depth and crustal basement thickness at rifted continental margins, which are substantially too great. The results from gravity anomaly inversion are dependent on the age of continental breakup due to the lithosphere thermal gravity anomaly correction being dependent on the lithosphere thermal re-equilibration time. Some papers consider the age of breakup for the west Iberian margin to be at the Aptian-Albian boundary, 112 Ma (Péron-Pinvidic *et al.* 2007); whereas others consider an older breakup age of 126 Ma, (Russell & Whitmarsh 2003; Manatschal 2004). As the gravity anomaly inversion requires a definitive breakup age, a Cretaceous breakup age of 120 Ma, which is within this proposed range, has been used. Changing the breakup age used within the gravity anomaly inversion to the maximum breakup age proposed, 126 Ma, or to the minimum breakup age proposed, 112 Ma, has a small effect on the results, but does not substantially change the overall conclusions. A more detailed description of the gravity anomaly inversion technique methodology is given in Greenhalgh & Kusznir (2007), Alvey *et al.* (2008), Chappell & Kusznir (2008) and Cowie & Kusznir (2012).

Within the gravity anomaly inversion the reference Moho depth is an important parameter that requires careful consideration and calibration. The 3-D gravity anomaly inversion technique determines 3-D Moho relief; the absolute Moho depth requires, in addition, a reference datum which is the reference Moho depth. The long wavelength components of the Earth's gravity anomaly field are controlled by deep mantle dynamic processes and are not related to lithosphere and crustal structure, and as a consequence the reference Moho depth varies globally. It is therefore necessary for the reference Moho depth to be determined by calibration against seismic refraction Moho depths to ensure the correct reference Moho depth is used within the gravity anomaly inversion (Cowie & Kusznir 2012); within this paper calibration has only been done using seismic refraction Moho depths for unequivocal oceanic crust. A crustal basement density of 2850 kg m^{-3} (Carlson & Herrick 1990; Christensen & Mooney 1995) and a mantle density of 3300 kg m^{-3} (Jordan & Anderson 1974) are used in the gravity anomaly inversion; sensitivity tests to these values have been made and do not significantly change the conclusions.

Reference Moho depths have been calibrated, for the oceanic domain, using profile IAM9, which has reliable seismic oceanic Moho depth estimates from the wide angle seismic data of Dean *et al.* (2000). Sensitivities to reference Moho depths of 37.5, 40 and 42.5 km have been examined for the IAM9 profile. Moho depths predicted from gravity anomaly inversion produced for these sensitivities to reference Moho depth are shown in Fig. 2(b). A reference Moho depth of 37.5 km is too small as it predicts Moho depths which are too shallow and in places plot above the top basement within the sedimentary layer. A larger reference Moho depth is required; both reference Moho depths of 40 km and 42.5 km predict a deeper Moho. Calibration gives a reference Moho depth of 41 km (inset of Fig. 2b) in order to predict crustal basement thicknesses consistent with those seen in the wide-angle seismic data.

The gravity anomaly inversion, which is carried out in the 3-D spectral domain, uses 3-D bathymetry and free air gravity anomaly data, while the sediment thicknesses are derived from the 2-D seismic profiles and are interpolated between profiles in order to construct a pseudo 3-D sediment volume. The results from the 3-D gravity anomaly inversion are then extracted along the 2-D profiles.

A crustal cross section (A–A′) along profile IAM9 (Fig. 2c), has been constructed using the bathymetry and 2-D sediment thickness data (Dean *et al.* 2000) with the crustal basement thicknesses and Moho depths predicted from gravity anomaly inversion assuming the calibrated reference Moho depth of 41 km. The crustal cross section along profile IAM9 (A–A′) shows the distribution of oceanic and continental crust and hence the structure of the OCT. The red dashed line shows the 7.9 km s^{-1} iso-velocity contour (Dean *et al.* 2000) representing the seismic Moho depth. There is a good correlation between the Moho depths predicted from gravity anomaly inversion, using the calibrated reference Moho depth of 41 km, and the seismic Moho depths; crustal basement thicknesses between 5 km and 7 km are predicted at the western end of the profile. In the centre of the profile (between 100 and 200 km) the crustal basement thicknesses predicted from gravity anomaly inversion thin considerably, to between approximately 1.5 and 2 km, and the gravity anomaly inversion predicts a shallower Moho depth than predicted by the 7.9 km s^{-1} iso-velocity contour. The start of the necking zone again shows a good correlation between the Moho depths predicted from gravity anomaly inversion and the seismic Moho depths. Under the continental crust inboard of the necking zone there is a significant difference between the gravity anomaly inversion predicted Moho depths and the Moho depths predicted by Dean *et al.* (2000). The difference, in part, can be attributed to a too thin estimate of sediment thickness in this region used within our gravity anomaly inversion, which results in the gravity anomaly inversion predicted Moho being too deep. (Dean *et al.* 2000) states that the crustal thicknesses at the continental end of the profile are from 2-D modelling of shipboard gravity data and their shallower Moho could also be the result of using lower crustal basement densities than those used within our gravity anomaly inversion.

The distribution of continental lithosphere thinning predicted from gravity anomaly inversion has also been used along the west Iberian rifted continental margin. During continental rifting and breakup there can be a significant addition of magmatic material to the crust. The thickness of the crustal magmatic addition is estimated using the parametrization of decompression melting model of White & McKenzie (1989), from the continental lithosphere thinning factor (γ) determined from gravity anomaly inversion, where

$$\gamma = 1 - \frac{1}{\beta}. \tag{1}$$

This parametrization of decompression melting is described in detail in Chappell & Kusznir (2008). Decompression melting results in magmatic addition, which leads to the generation of oceanic crust and also magmatic underplating and extrusives, for example seaward dipping reflectors (SDRs) at many rifted continental margins (at the west Iberian margin SDRs are not observed). 'Normal' decompression melting produces a 7-km-thick oceanic crust with the initiation of decompression melting occurring at $\gamma = 0.7$ and a maximum magmatic addition of 7 km at a thinning factor of 1.0 (for $\beta = \infty$). We also consider the case of a magma-starved margin where no magmatic addition to the crust is generated. In the case of magma-starved margins, serpentinization of exhumed mantle occurs. Therefore, we also consider a solution for mantle serpentinization, applicable to magma-starved margins, in which serpentinization begins at approximately $\gamma = 0.7$ (corresponding to approximately 10-km-thick crust) and at $\gamma = 1.0$ generates a

serpentinized mantle with a mass deficiency with respect to mantle equivalent to crustal basement of thickness 3 km. This estimate of the equivalent mass deficiency of serpentinized mantle is described in the Appendix.

Continental lithosphere thinning factor (γ) estimates for profile IAM9, derived from gravity anomaly inversion assuming three different solutions, are shown in Fig. 2(d). A magma-starved solution; a 'normal' magmatic solution and a solution for serpentinized mantle have been examined. Continental lithosphere thinning factors of zero indicate that there has been no stretching or thinning of the continental lithosphere, whereas a continental lithosphere thinning factor of one indicates that there has been infinite stretching and thinning of the original continental lithosphere and there is no continental lithosphere (or crust) remaining. Changes in the continental lithosphere thinning factors, determined from gravity anomaly inversion, specifically changes from high thinning factors (between 0.9 and 1.0) to lower thinning factors, may be used to constrain the COB and necking zone location along the profile lines. Along profile IAM9 (Fig. 2d), the continental lithosphere thinning factors from gravity anomaly inversion for 'normal' magmatic addition are 1.0 along most of the profile (they begin to decrease at approximately 260 km distance along profile); this solution probably places the COB too far inboard and is inappropriate for a magma-starved margin. The magma-starved solution, with no serpentinization, fails to reach 1.0 anywhere. The serpentinized mantle solution predicts high continental lithosphere thinning factors in the central region, which is where Dean *et al.* (2000) indicate that there are peridotite mantle ridges. The interpretation of these continental lithosphere thinning factor curves to constrain COB location and the presence of exhumed mantle or 'normal' oceanic crust is discussed in detail in Section 5.

2.2 RDA analysis: profile IAM9

2.2.1 Sediment corrected RDA

RDA analysis has been applied to the west Iberian rifted continental margin in order to examine OCT bathymetric anomalies with respect to expected oceanic bathymetries at the rifted continental margin. A RDA for oceanic crust is the difference between observed (b_{obs}) and ocean age predicted bathymetry ($b_{\mathrm{predicted}}$). Age predicted bathymetries have been calculated using the thermal plate model predictions from Crosby & McKenzie (2009). Sensitivities to the thermal plate model predictions from Parsons & Sclater (1977) and Stein & Stein (1992) have also been examined (Fig. 3b); RDA results computed using these different thermal plate model predictions do not vary significantly.

$$\mathrm{RDA} = b_{\mathrm{obs}} - b_{\mathrm{predicted}}. \tag{2}$$

Changes in RDA signature are used to estimate the distal extent of continental crust and where unequivocal oceanic crust begins.

Sediment corrected bathymetry, used to calculate RDAs corrected for sediment loading, has been determined using flexural backstripping and decompaction. Fig. 3(c) shows a comparison of the uncorrected RDA and the sediment corrected RDA along profile IAM9. Correcting for the effect of sediment loading has a considerable effect on the RDA results; the difference between the uncorrected RDA and the sediment corrected RDA is approximately 1500 m at the western end of the profile. Sediment corrected bathymetry has been calculated using flexural backstripping (Kusznir *et al.* 1995) and comprises the removal of the sedimentary load, allowing for the flexural isostatic response and decompaction of the remaining sediments. Flexural backstripping and decompaction assumes shaly-sand compaction parameters (Sclater & Christie 1980) during the removal of the sedimentary layer. Removal of the sedimentary layer along profile IAM9, results in a sediment corrected bathymetry that is approximately 1500 m deeper than observations of present day bathymetry. The sediment corrected RDA along profile IAM9 (Fig. 3c), is negative with a magnitude between −1000 and −1500 m at the western end of the profile.

Age predicted oceanic bathymetries, used to calculate the sediment corrected RDA, are dependent on the oceanic lithospheric age. The Müller *et al.* (2008) global ocean age isochrons do not extend the entire length of profile IAM9; it is therefore necessary to consider sensitivities to oceanic lithospheric age. Two approaches have been examined: the first uses a constant value of 120 Ma for the profile, whilst the second uses Müller *et al.* (2008) age isochrons with their age gradient extrapolated inboard. A comparison and sensitivity of the sediment corrected RDA results to ocean age isochrons is shown in Fig. 3(d), both approaches produce similar results.

The flexural backstripping process calculates the flexural isostatic response of the removed layer of sediments. Within this calculation the effective elastic thickness (T_{e}) controlling the flexural strength of the lithosphere is considered. T_{e} depends on the bending stresses applied to the plate, the rate of stress application, the lithosphere composition and the geothermal gradient (Kusznir & Karner 1985). T_{e}'s between 1.5 and 5 km have been determined for syn-rift extensional settings (Roberts *et al.* 1998). For post-rift flexural isostatic response, Roberts *et al.* (1998) show that this is relatively insensitive to the magnitude of T_{e} because of the longer wavelength of post-rift sediment loading compared to syn-rift. The sensitivity to T_{e} is shown for the Iberian Abyssal Plain sediment corrected RDA results in Fig. 3(e); sensitivities to T_{e}'s of 1.5, 5 and 10 km have been examined. T_{e}'s of 1.5, 5 and 10 km produce sediment corrected RDAs of similar magnitude; a T_{e} of 1.5 km has been used due to the negligible difference in the magnitude of the sediment corrected RDAs.

2.2.2 RDA component from crustal basement thickness variations ($\mathrm{RDA_{CT}}$)

In addition to the RDA corrected for sediment loading, the RDA component from variations in crustal basement thickness ($\mathrm{RDA_{CT}}$) has also been computed, which is the result of the presence of anomalously thick or thin crust. Crustal basement thicknesses from gravity anomaly inversion (using reference Moho depth calibrated against seismic Moho depths) are used to predict departures from the average global oceanic crustal thickness of 7 km (White *et al.* 1992). $\mathrm{RDA_{CT}}$ has been computed using the difference between the gravity anomaly inversion predicted crustal basement thickness (tc_{grav}) and the average global oceanic crustal basement thickness (tc_{ref}) together with Airy isostasy. The local isostatic response to variation in gravity inverted non-continental crustal thickness, from the 7 km global average oceanic crustal thickness (tc_{ref}) is given by:

$$\mathrm{RDA_{CT}} = \frac{(tc_{\mathrm{ref}} - tc_{\mathrm{grav}})(\rho_{\mathrm{m}} - \rho_{\mathrm{c}})}{(\rho_{\mathrm{m}} - \rho_{\mathrm{infil}})}, \tag{3}$$

where ρ_{m} is the density of the mantle (3300 kg m^{-3}), ρ_{c} is the density of the crust (2850 kg m^{-3}) and ρ_{infill} is the density of the water infill (1000 kg m^{-3}). Crust, which is approximately 7 km thick, will have a corresponding $\mathrm{RDA_{CT}}$ of zero. A positive $\mathrm{RDA_{CT}}$ reflects crust that is thicker than 7 km, whereas if the $\mathrm{RDA_{CT}}$ is

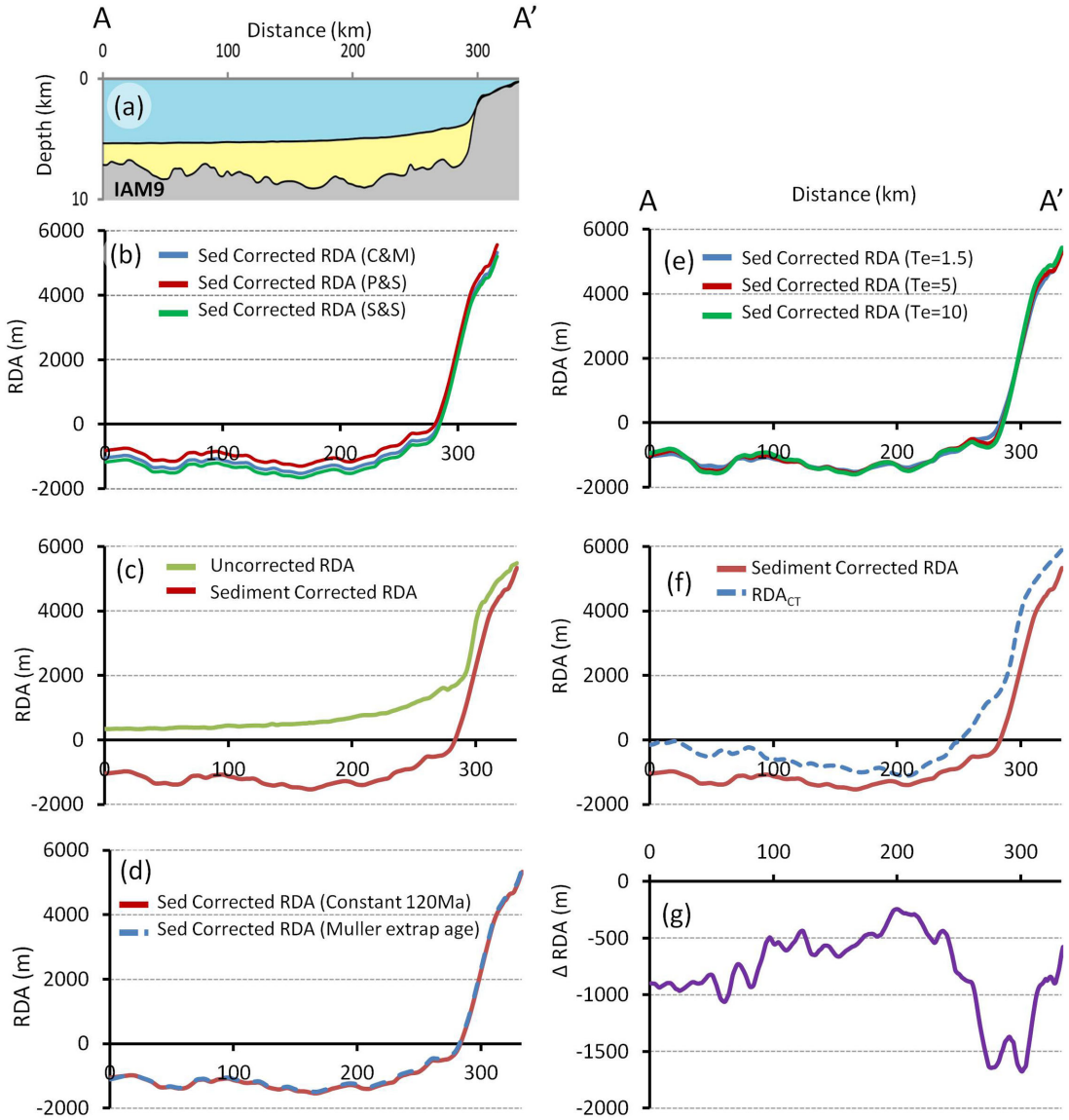

Figure 3. (a) Bathymetry and depth to top basement for IAM9 profile. (b) Comparison of the residual depth anomaly (RDA) results computed using bathymetry-age predictions from Crosby & McKenzie (C&M; 2009), Parsons & Sclater (P&S; 1977) and Stein & Stein (S&S; 1992). (c) Comparison of uncorrected RDA results with the sediment corrected RDA results along IAM9. (d) The sensitivity to oceanic lithospheric age for sediment corrected RDA results examined using two approaches: the first uses a constant value of 120 Ma for the profile, whilst the second uses Müller *et al.* (2008) age isochrons with their age gradient extrapolated inboard. (e) Sensitivities to the effective elastic thickness (T_e) for the sediment corrected RDA results. (f) Comparison of sediment corrected RDA and the RDA component from crustal thickness variations (RDA$_{CT}$) along IAM9. (g) RDA corrected for sediment loading and crustal thickness variation.

negative, this corresponds to crust that is thinner than 7 km or the presence of exhumed mantle.

The RDA$_{CT}$ along profile IAM9 (Fig. 3f) ranges between zero and approximately −800 m at the western end and central region of the profile, and becomes more negative before increasing and becoming positive over the continental crust.

2.2.3 Comparison of sediment corrected RDA with RDA component from crustal basement thickness variations

Fig. 3(f) shows the sediment corrected RDA and the RDA$_{CT}$ along profile IAM9. In oceanic regions it is expected that the RDA signal, from both the sediment corrected RDA and the RDA$_{CT}$, will be constant and near zero, whereas for regions of thicker continental crust inboard of the COB, it is expected that the RDA signals will become more positive. Changes in the RDA signal may be used to identify the change in crustal mass deficiency and thickness with respect to the mantle; these changes in RDA signal may also be interpreted as a change in crustal type enabling the determination of the COB location.

Both the sediment corrected RDA and the RDA$_{CT}$ along profile IAM9 are negative in the western and central region and show the same general trend along the profile although they have different magnitudes. The difference (ΔRDA) between the sediment corrected RDA and the RDA$_{CT}$ corresponds to the RDA corrected for both sediment loading and variations in crustal thickness away from the oceanic average.

$$\Delta\text{RDA} = \text{sediment corrected RDA} - \text{RDA}_{CT}. \quad (4)$$

A ΔRDA of zero implies that there is no anomalous uplift or subsidence at the margin, whereas a positive ΔRDA implies anomalous uplift and a negative ΔRDA implies anomalous subsidence along a margin. The ΔRDA (Fig. 3g) along IAM9 is between −300 and −1000 m at the western end of the profile, which is equated to mantle dynamic subsidence.

2.3 Continental lithosphere thinning from subsidence analysis

Subsidence analysis has been used to determine the distribution of continental lithosphere thinning and the distal extent of continental crust in order to locate the inner and outer bounds of the OCT. Subsidence analysis involves the conversion of water loaded subsidence into continental lithosphere thinning factors, assuming McKenzie (1978). Flexural backstripping is used to give the sediment corrected bathymetry to top pre-rift and top oceanic crust (Fig. 4b). It is assumed that the initial datum of original continental pre-rift surface was at or near to sea level; therefore the sediment corrected bathymetry can be equated to water loaded subsidence (see comparable estimate of tectonic subsidence from Henning *et al.* 2004). Water loaded subsidence is interpreted as the sum of initial (Si) and thermal (St) subsidence in the context of the McKenzie (1978) intracontinental rift model. A correction for magmatic addition due to adiabatic decompression (White & McKenzie 1989) during continental rifting and seafloor spreading has been included (see Roberts *et al.* 2013) and uses the same scheme as described earlier in the gravity anomaly inversion section. Magmatic addition from decompression melting results in thicker crust due to volcanic intrusion and extrusion, which isostatically reduces the initial subsidence as predicted by McKenzie (1978) and corresponds to the formation of oceanic crust. Magmatic addition also increases the thickness of the crust thinned by lithosphere stretching.

Initial subsidence corresponds to the isostatic response of the crustal thinning and thermal loads at the time of rifting, which is assumed to be instantaneous; whilst total subsidence corresponds to the isostatic response of the crustal thinning and thermal loads after a defined time in the post-rift. Sensitivity tests using upper and lower bounds of the time of breakup (126 and 112 Ma) have been examined and the results are not significantly different. The crustal thinning load is assumed to be constant after rifting, while the thermal subsidence varies with time due to the dissipation of the syn-rift lithosphere thermal anomaly. Instantaneous rifting is assumed, which allows the comparison of the numerically calculated total subsidence from flexural backstripping with that analytically calculated using McKenzie (1978) modified for magmatic additions. Magmatic additions due to decompression melting modify the predicted relationship between continental lithosphere thinning factor (γ) and water loaded subsidence. Water loaded subsidence is inverted using the 'normal' magmatic curve (Fig. 4c) magma poor and serpentinized mantle curves (Fig. 4d) to give continental lithosphere thinning factors. The subsidence analysis methodology assumes depth uniform stretching and thinning, as a consequence thinning factors for continental lithosphere and crust are identical. The isostatic response of mantle serpentinization is described in the Appendix, and is estimated to be equivalent to crustal basement of approximately 3 km thickness.

Continental lithosphere thinning factors from subsidence analysis along profile IAM9 are shown in Fig. 4(e). For the west Iberian margin, a 'normal' magmatic solution, a magma-starved solution

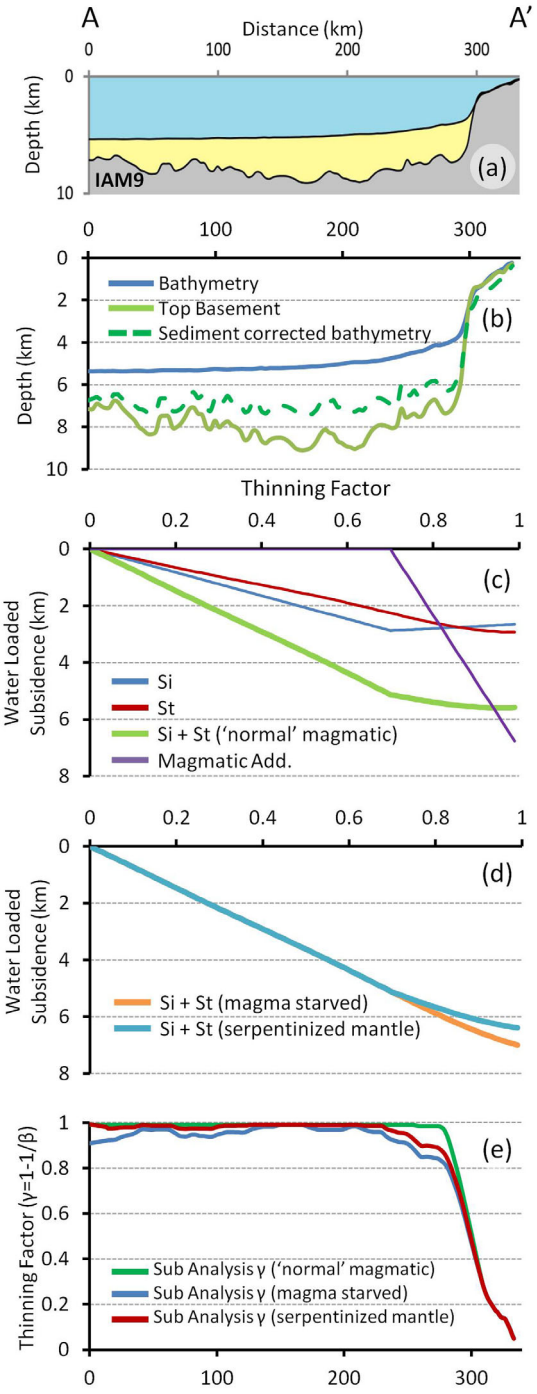

Figure 4. Subsidence analysis involves the conversion of water loaded subsidence into continental lithosphere thinning factors, assuming McKenzie (1978), and is modified to incorporate the isostatic consequence of magmatic addition. (a) Bathymetry and depth to top basement for IAM9 profile. (b) Sediment corrected bathymetry determined by flexural backstripping of section (a). (c) Water loaded subsidence as a function of lithosphere thinning factor (γ) for a 'normal' magmatic solution. Initial subsidence (Si) is shown in blue, the time dependent thermal subsidence (St) is shown in red, the combined total subsidence (Si+St) is shown in green and the magmatic addition assuming decompression melting producing oceanic crust of 7 km is shown in purple. (d) Water loaded subsidence as a function of lithosphere thinning factor (γ) for a magma-starved and a serpentinized mantle solution. (e) Continental lithosphere thinning factors (γ) from subsidence analysis along IAM9. Sensitivities to a 'normal' magmatic solution, a magma-starved solution and a solution for serpentinized mantle are shown.

and a solution for serpentinized mantle are examined. A 'normal' magmatic solution predicts continental lithosphere thinning factors of 1.0 everywhere outboard of the necking zone, while the magma-starved solution, with no serpentinization, predicts continental lithosphere thinning factors between 0.8 and 1. The solution for serpentinized mantle lies between these two and is more appropriate to a magma poor margin. Continental lithosphere thinning factors derived from subsidence analysis can be used to determine COB location and crustal type which is discussed in Section 5.

Continental lithosphere thinning factors predicted from gravity anomaly inversion are generally less than those predicted from subsidence analysis. This difference can be attributed to dynamic topography, as the gravity anomaly inversion results have been calibrated and include a correction for dynamic topography, whereas the subsidence analysis results do not.

The subsidence analysis for IAM9 by Henning *et al.* (2004) uses a different approach, predicting crustal thickness variation; as a consequence our results are not easily compared.

3 OCT STRUCTURE ALONG THE LUSIGAL 12 PROFILE

3.1 Crustal basement thickness and continental lithosphere thinning along Lusigal 12 from gravity anomaly inversion

Gravity anomaly inversion has been applied to the Lusigal 12 profile [with the TGS extension; see Sutra *et al.* (2013)] in order to determine the crustal basement thickness, Moho depth and continental lithosphere thinning along profile. Within the gravity anomaly inversion the calibrated reference Moho depth of 41 km, from IAM9, has been assumed to be applicable due to the proximity of Lusigal 12 to IAM9. Crustal cross section (B–B′) along profile Lusigal 12 (Fig. 5b) is constructed using bathymetry, sediment thickness (Sutra & Manatschal 2012; Fig. 5a) and predicted Moho depths from gravity anomaly inversion. Using the calibrated reference Moho depth of 41 km, the gravity anomaly inversion predicts thin crust of between 2 and 4 km thickness at the western end of the profile.

Continental lithosphere thinning factors (γ) predicted from gravity anomaly inversion are shown in Fig. 5(c). Sensitivities to a magma-starved solution, a 'normal' magmatic solution and a solution for serpentinized mantle have been examined. Continental lithosphere thinning factors from gravity anomaly inversion show high thinning factors for all three solutions at the western end of the profile. Continental lithosphere thinning factors for a 'normal' magmatic solution saturate at 1.0 in the central and western section of the profile. If a 'normal' magmatic solution is applicable to this profile, it suggests that this region is all oceanic. Continental lithosphere thinning factors for a serpentinized mantle solution reach 1.0 at the western end of the profile, which implies the presence of exhumed mantle. The magma poor solution predicts continental lithosphere thinning factors of 0.9 for the same region.

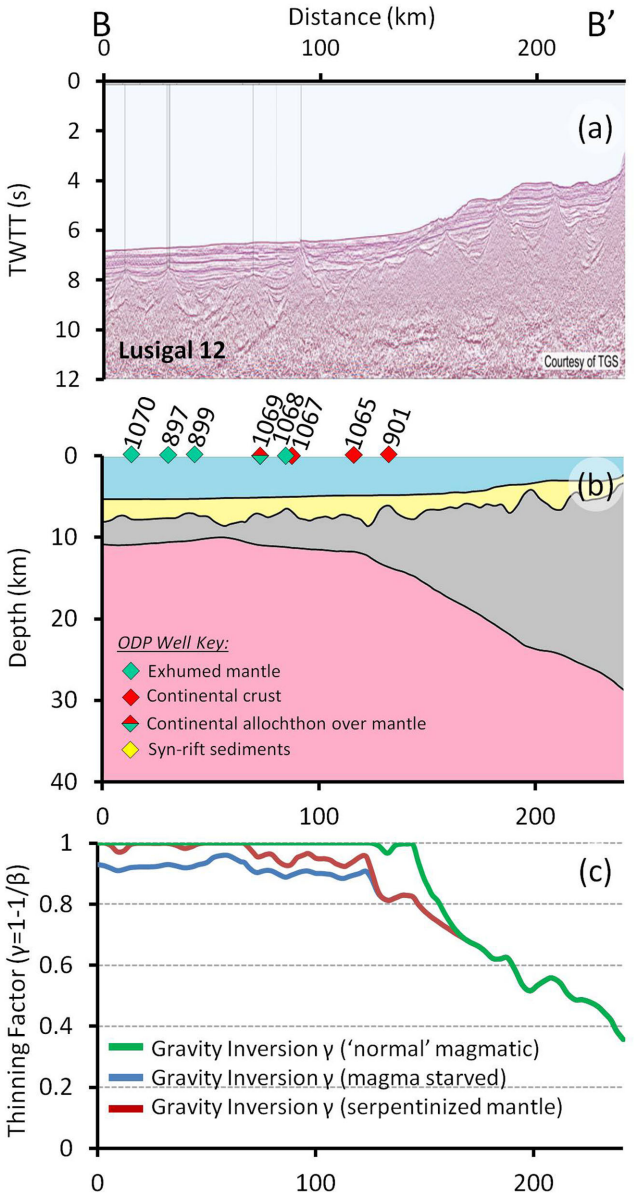

Figure 5. (a) 2-D seismic reflection profile (Sutra & Manatschal 2012) for Lusigal 12 (with the TGS extension). (b) Crustal cross section B–B′ across Iberian Abyssal Plain, from gravity anomaly inversion. ODP well locations are identified and colour coded by crustal basement type. (c) Continental lithosphere thinning factors (γ) predicted from gravity anomaly inversion along Lusigal 12. Sensitivities to a 'normal' magmatic solution, a magma-starved solution and a solution for serpentinized mantle are shown.

3.2 RDAs corrected for sediment loading and crustal basement thickness variations along Lusigal 12

Sediment corrected RDAs and RDA_{CT} have been computed along the Lusigal 12 profile as shown in Fig. 6(b) and show the same general trend, however, with varying magnitudes. The sediment corrected RDA ranges between −500 and −1500 m in the west, implying that the presence of crust which is thinner than 7 km or anomalous subsidence. At the western end of the profile, the RDA_{CT} ranges between −800 and −1000 m, corresponding to either the presence of crust which is thinner than 7 km, or the presence of exhumed mantle. Fig. 6(c) shows the ΔRDA plot for Lusigal 12, which illustrates the sediment corrected RDA further corrected for crustal basement thickness variations. The ΔRDA ranges between zero and −500 m implying that there is anomalous subsidence along

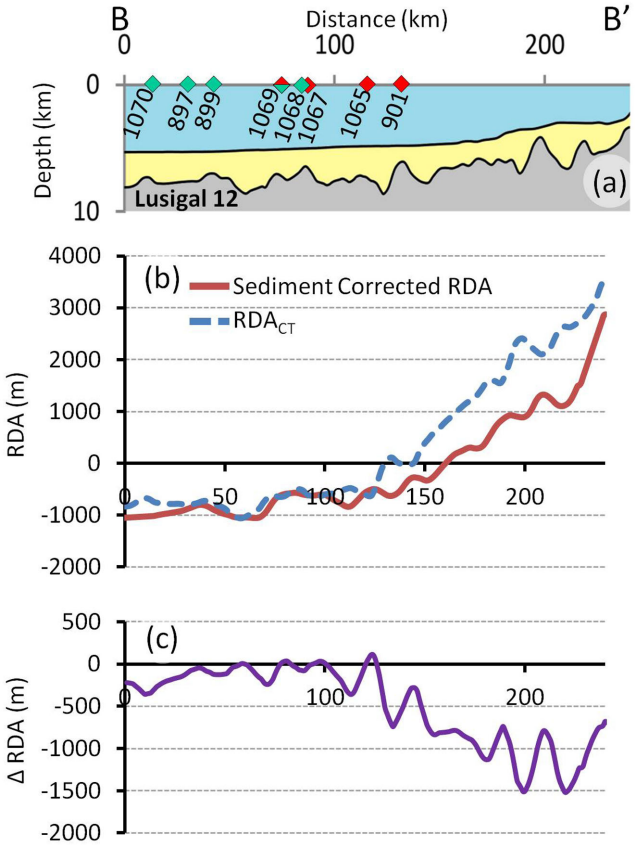

Figure 6. (a) Bathymetry and depth to top basement for Lusigal 12. ODP well locations are identified and colour coded by crustal basement type (see ODP well key on Fig. 5b). (b) Sediment corrected RDA and the RDA component from crustal thickness variations (RDA$_{CT}$) along Lusigal 12. (c) RDA corrected for sediment loading and crustal thickness variations.

Lusigal 12, which is in agreement with the anomalous subsidence predicted by RDA analysis along profile IAM9, the other profile in the Iberian Abyssal Plain.

3.3 Continental lithosphere thinning from subsidence analysis along Lusigal 12

Continental lithosphere thinning factors determined from subsidence analysis are shown in Fig. 7(b); at the western end of the Lusigal 12 profile, continental lithosphere thinning factors from subsidence analysis are between 0.85 and 1.0, indicative of oceanic crust or possibly exhumed mantle. Sensitivities to the three magmatic solutions have been examined. Assuming a 'normal' magmatic solution, subsidence analysis predicts continental lithosphere thinning factors of 1.0 in the centre and western end of the profile, which for this magmatic assumption would indicate the presence of oceanic crust. The magma-starved solution with no serpentinization does not reach a continental lithosphere thinning factor of 1.0, except at the extreme western end of the profile. The solution assuming serpentinized mantle reaches thinning factors exceeding 0.95 for the western part of the profile. In Section 5, we discuss the interpretation of these continental lithosphere thinning factors to determine COB location and crustal type.

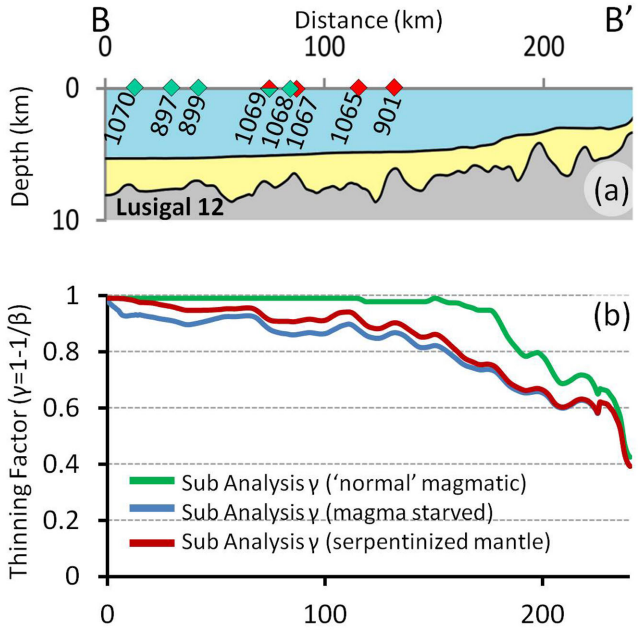

Figure 7. (a) Bathymetry and depth to top basement for Lusigal 12. ODP well locations are identified and colour coded by crustal type (see ODP well key on Fig. 5b). (b) Continental lithosphere thinning factors (γ) from subsidence analysis along Lusigal 12. Sensitivities to a 'normal' magmatic solution, a magma-starved solution and a solution for serpentinized mantle are shown.

4 OCT STRUCTURE ALONG PROFILE ISE-01

4.1 Crustal basement thickness and continental lithosphere thinning along ISE-01 from gravity anomaly inversion

Gravity anomaly inversion has been applied in order to determine crustal basement thickness, Moho depth and continental lithosphere thinning along profile ISE-01. Sediment thicknesses (Fig. 8a) used in the gravity anomaly inversion are from University of Texas Institute of Geophysics (UTIG) seismic database. Sensitivities to reference Moho depths have been examined within the gravity anomaly inversion along profile ISE-01, reference Moho depth sensitivities of 35, 37.5 and 40 km are shown in Fig. 8(b). A reference Moho depth of 35 km is too small and predicts a Moho which is too shallow and comes up into the sediments at the start of the profile, whereas both reference Moho depths of 37.5 and 40 km predict more sensible Moho depths; calibration of the reference Moho depth is therefore required. Zelt *et al.* (2003) uses first arrival seismic tomography and reflection tomography to investigate the seismic velocity structure of the ISE-01 profile. They show *P*-wave iso-velocity contours between 7 and 7.6 km s^{-1}, but are not able to resolve the expected higher seismic velocities consistent with rays sampling the mantle. Their seismic Moho based on first arrival seismic tomography and reflection tomography typically fall within the 7 and 7.6 km s^{-1} range, suggesting that their seismic Moho is too shallow. Calibration of Moho depths for the gravity anomaly inversion should only be done on unequivocal oceanic crust (or very well seismically constrained Moho depths beneath continental crust). ODP wells along ISE-01 do not observe oceanic crust, nor is there any well constrained seismic Moho, so calibration of the reference Moho depth for ISE-01, using seismic Moho depths has not been possible. As a

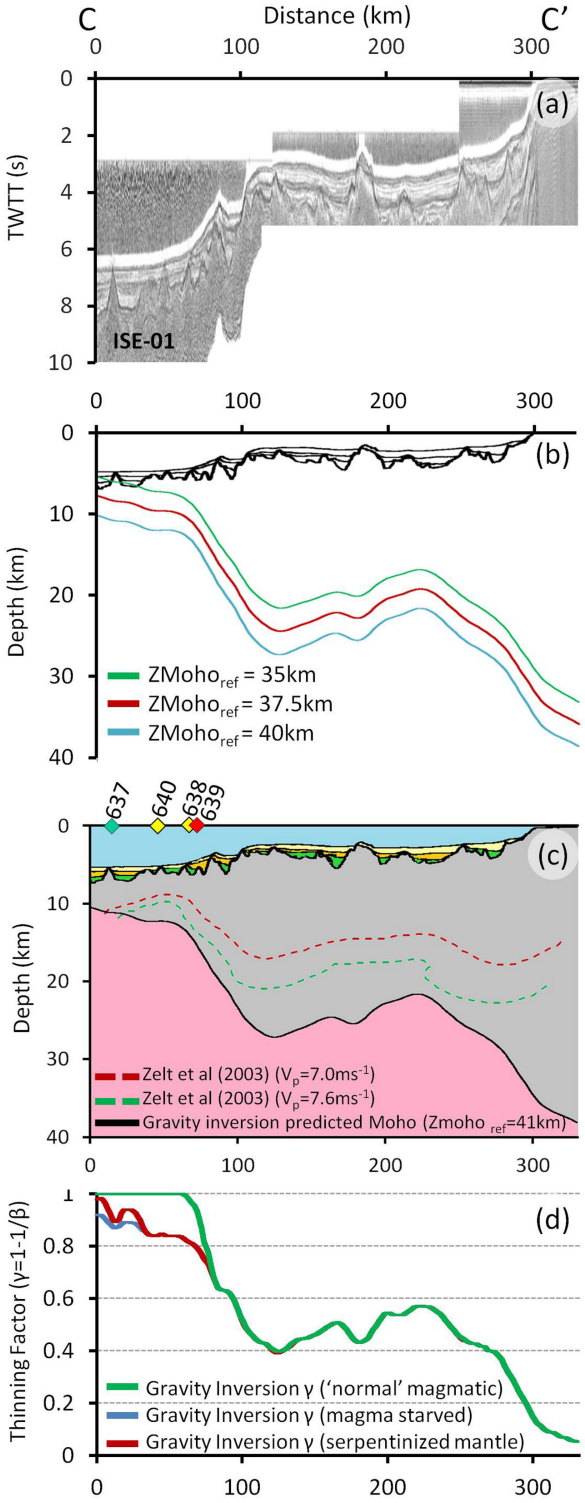

Figure 8. (a) 2-D seismic reflection data (from UTIG) along profile ISE-01. (b) Crustal cross section (C–C′) along ISE-01 showing Moho depths predicted from gravity anomaly inversion, using reference Moho depths of 35, 37.5 and 40 km. (c) Crustal cross section (C–C′) along profile ISE-01 using the calibrated reference Moho depth of 41 km. The red dashed line shows the 7.0 km s^{-1} iso-velocity contour and green dashed line shows the 7.6 km s^{-1} iso-velocity contour Zelt *et al.* (2003). ODP well locations are identified and colour coded by crustal basement type (see ODP well key on Fig. 5b). (d) Continental lithosphere thinning (γ) from gravity anomaly inversion along profile ISE-01. Sensitivities to a 'normal' magmatic solution, a magma-starved solution and a serpentinized mantle solution are shown.

consequence we have used the reference Moho depth of 41 km for the gravity anomaly inversion determined from profile IAM9.

Crustal cross section (C–C′) along ISE-01 (Fig. 8c) shows Moho depths from gravity anomaly inversion using the reference Moho depth of 41 km calibrated on line IAM9. The Moho depth from gravity inversion is substantially deeper than the Moho determined by Zelt *et al.* (2003) from seismic reflections. Sediment thicknesses used within the gravity anomaly inversion are derived from the seismic pick of top basement from ISE-01 reflection data. We note however that the seismic tomography from Zelt *et al.* (2003) shows upper crustal seismic velocities suggesting that there may be several kilometres of pre-rift sediments beneath the seismic reflection top basement for both the Galicia Interior Basin and Galicia Bank. Inclusion of a significant thickness of pre-rift sediments in the gravity anomaly inversion would give a shallower Moho, closer to that proposed by Zelt *et al.* (2003). Alternatively using a lighter crustal basement density would also result in a shallower Moho from the gravity inversion. The *P*-wave iso-velocity contours of 7 and 7.6 km s^{-1} from Zelt *et al.* (2003) are also shown on Fig. 8(c); the seismic tomography does not show seismic velocities typical of normal mantle. The seismic reflection Moho of Zelt *et al.* (2003) plots between these iso-velocity contours. We speculate that the reflection returns used by Zelt *et al.* (2003) to determine Moho depth may be from the top of a lower crustal intrusive body rather than from the top of the mantle. Whatever the cause of the difference between the gravity and seismic Moho depths under the Galicia Interior Basin and Galicia Bank, the calibration of reference Moho depth in the oceanic domain means that this problem as little effect on the gravity inversion results for the distal part of the margin.

Fig. 8(d) shows continental lithosphere thinning factor (γ) estimates from gravity anomaly inversion for profile ISE-01 assuming a magma-starved model; a 'normal' magmatic solution and a solution for serpentinized mantle. A 'normal' magmatic solution predicts continental lithosphere thinning factors of 1.0 at the western end of the profile. A magma-starved solution, with no serpentinization predicts continental lithosphere thinning factors that do not reach 1.0 anywhere. A solution for serpentinized mantle shows continental lithosphere thinning factors reaching 1.0 at the extreme western end of the profile.

4.2 RDAs corrected for sediment loading and crustal basement thickness variations along ISE-01

At the western end of the ISE-01 profile, the sediment corrected RDA ranges between zero and −800 m (Fig. 9b), which implies either the presence of crust, which is thinner than 7 km or anomalous subsidence. The RDA$_{CT}$ ranges between zero and −1000 m (Fig. 9b), which corresponds to the presence of crust which is thinner than 7 km, or the presence of exhumed mantle. The sediment corrected RDA and the RDA$_{CT}$ along profile ISE-01 (Fig. 9b) show the same general trend. The sediment corrected RDA further corrected for variations in crustal basement thickness (ΔRDA; Fig. 9c) is approximately zero implying that there is negligible anomalous subsidence or uplift to the west of Galicia Bank.

4.3 Continental lithosphere thinning from subsidence analysis along ISE-01

Subsidence analysis using a 'normal' magmatic solution predicts continental lithosphere thinning factors of 1.0 at the western end of the profile (Fig. 10b). The magma-starved solution with no

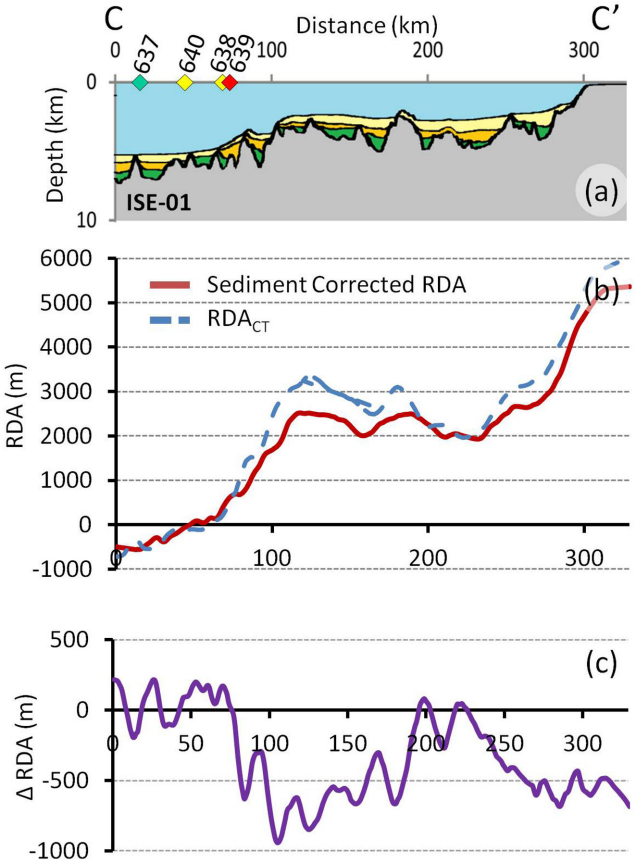

Figure 9. (a) Bathymetry and depth to top basement for the ISE-01 profile. ODP well locations are identified and colour coded by crustal basement type (see ODP well key on Fig. 5b). (b) Sediment corrected RDA and the RDA component from crustal thickness variations (RDA$_{CT}$) along ISE-01. (c) RDA corrected for sediment loading and crustal thickness variations.

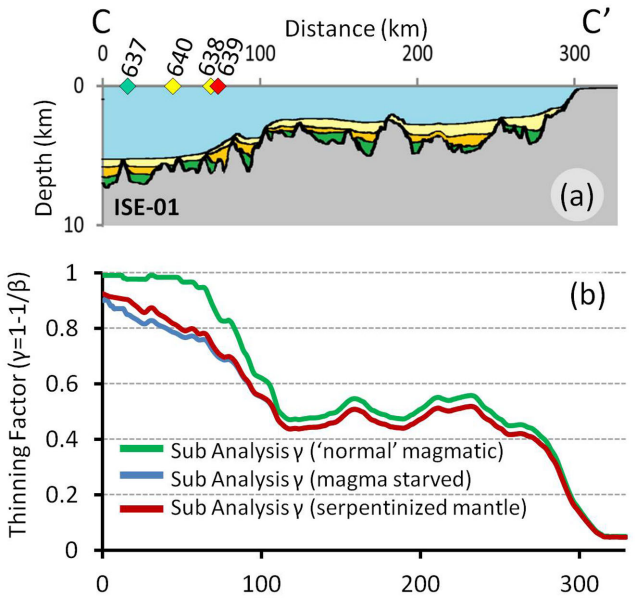

Figure 10. (a) Bathymetry and depth to top basement for the ISE-01 profile. ODP well locations are identified and colour coded by crustal basement type (see ODP well key on Fig. 5b). (b) Continental lithosphere thinning factors (γ) from subsidence analysis along ISE-01. Sensitivities to a 'normal' magmatic solution, a magma-starved solution and a solution for serpentinized mantle are shown.

serpentinization, nor the solution for serpentinized mantle, reach continental lithosphere thinning factors of 1.0; maximum values reached are 0.9.

5 PREDICTING OCT STRUCTURE AND COB LOCATION

The previous sections have shown the results from integrated quantitative analysis using gravity anomaly inversion, RDA and subsidence analysis, applied to IAM9 and Lusigal 12 in the Iberian Abyssal Plain and ISE-01 on Galicia Bank. The results from each of these techniques may be used to assist in understanding the transition from continental to oceanic crust; however, it is preferable that the results from each technique should to be examined together. For each of the three profiles considered, a composite analysis plot is used to summarize the results from gravity anomaly inversion, RDA and subsidence analysis, as shown in Figs 11–13. The composite analysis plot consists of (i) a crustal cross section from gravity anomaly inversion, (ii) sediment corrected RDA and RDA$_{CT}$ along profile and (iii) a comparison of the continental lithosphere thinning factors predicted from gravity anomaly inversion and subsidence analysis. The analysis of the composite plot allows for an informative interpretation of the OCT structure, COB location and crustal type to be made, when the crustal domains are clearly defined. Using ODP wells, located along the Lusigal 12 and ISE-01 profiles, we compare the predicted OCT structure and COB location determined from integrated quantitative analysis with that inferred from direct well observations.

Table 1 summarizes the crustal types encountered along the western Iberian profiles and the consequent ranges of crustal basement thicknesses, continental lithosphere thinning factors and RDA results predicted from the integrated analysis techniques that we would expect to see in each of these domains. We use a crustal thickness of 10 km to mark the transition from the necking zone to hyper-extended continental crust (consistent with Aslanian *et al.* (2009)). The interpreted boundaries between each of these crustal types are based on these values (Table 1) and correspond to changes in crustal basement thickness from gravity anomaly inversion, variations in the RDA signal from the sediment corrected RDA and RDA$_{CT}$, and changes in continental lithosphere thinning factors derived from subsidence analysis and gravity anomaly inversion. Whilst we use the values in Table 1 for the results from each analytical technique to identify the various crustal domain along profile and locate the boundaries between these different crustal types, when considering all the techniques together there are discrepancies between the predicted locations of these boundaries. The transitional nature of these boundaries may in part explain these discrepancies. In our interpretation, we first picked the boundaries using the results from each individual technique and then considered all the techniques together so that our boundaries reflect the 'best-fit' from the integrated approach.

5.1 IAM9

The composite analysis plot for profile IAM9 in the Iberian Abyssal Plain (Fig. 11) is interpreted as showing three distinct crustal types: oceanic crust (zone A), serpentinized exhumed mantle (zone B) and continental crust which can be further subdivided into hyper-extended continental crust (zone C), the crustal necking zone (zone D), and proximal continental crust (zone E). We have examined the relationship between our interpretations of the boundaries

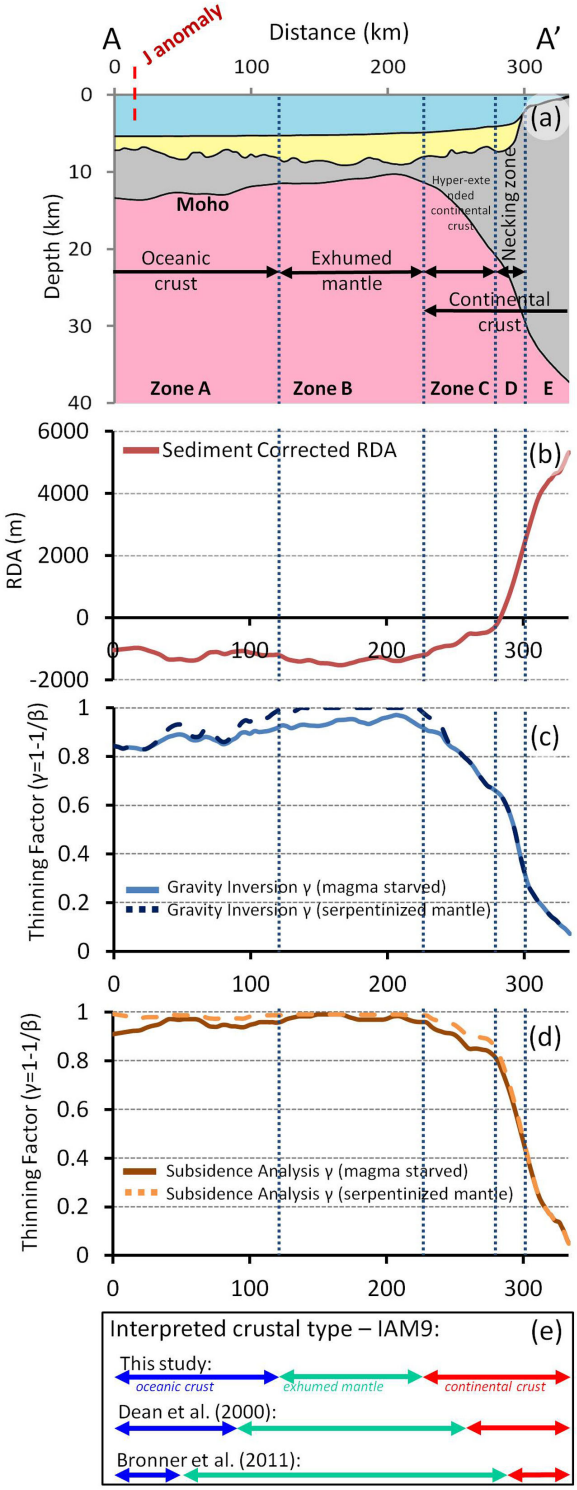

Figure 11. Composite analysis plot along IAM9, showing interpretations of crustal basement types made from the integrated quantitative analysis. (a) Crustal cross section along profile IAM9 (A–A′) from gravity anomaly inversion. The location of the J anomaly is indicated in red. (b) Sediment corrected RDA along IAM9. (c) Continental lithosphere thinning factors (γ) from gravity anomaly inversion assuming a magma-starved and a serpentinized mantle solution. (d) Continental lithosphere thinning factors (γ) from subsidence analysis assuming a magma-starved and a serpentinized mantle solution. Our interpreted boundaries between the crustal zones are indicated by the dashed lines. (e) Comparison of our interpreted crustal types with those from Dean *et al.* (2000) and Bronner *et al.* (2011).

between these three crustal types to those proposed in the literature, in particular the J anomaly. The J anomaly is a structural ridge or step in the oceanic basement that lies beneath the J magnetic anomaly (Tucholke & Ludwig 1982). Whilst the J anomaly and the interfaces between the crustal zones are shown as sharp lines, in reality they are likely to be transitional boundaries. The J anomaly is identified at approximately 25 km distance along the IAM9 profile (Fig. 11a; Dean *et al.* 2000; Whitmarsh *et al.* 2001; Bronner *et al.* 2011), and corresponds to inflection points in Moho depth, RDA and continental lithosphere thinning factors, determined assuming a magma-starved solution, and is west of our interpreted COB.

The discussions below refer to Fig. 11, unless otherwise stated.

5.1.1 Zone A: oceanic crust

In zone A, the crustal basement thicknesses from gravity anomaly inversion are between 6 and 7 km. The negative sediment corrected RDA is indicative of crust which is thinner than 7 km or anomalous subsidence, whilst the negative RDA_{CT} (shown in Fig. 3f) corresponds to the presence of thin crust derived from gravity anomaly inversion. The continental lithosphere thinning factors in zone A derived from gravity anomaly inversion and subsidence analysis using a 'normal' magmatic solution are 1.0 (shown in Figs 2d and 4e), implying the presence of oceanic crust.

If a magma-starved or a serpentinized mantle solution is assumed, the continental lithosphere thinning factors do not reach 1.0 from both gravity anomaly inversion and subsidence analysis, which implies thin continental crust. In zone A, a 'normal' magmatic solution is preferred as it produces high thinning factors of 1.0 which, together with crustal basement thicknesses between 6 and 7 km, we interpret as indicators for the presence of oceanic crust, consistent with the literature.

The interface between zones A and B corresponds to the boundary between oceanic crust and serpentinized exhumed mantle and is located by changes in Moho depth, RDAs and continental lithosphere thinning factors determined assuming magma-starved or a serpentinized mantle solution.

5.1.2 Zone B: exhumed mantle

In zone B, the crustal basement thicknesses decrease from 7 km in the west to approximately 3 km at the eastern end of the zone. These very low values of crustal thicknesses are apparent crustal thicknesses derived from the mass deficiency of serpentinized exhumed mantle with respect to unserpentinized mantle below (see the Appendix). Thicknesses of 3 km or less are indicative of the presence of serpentinized exhumed mantle; the very low crustal thicknesses derived from gravity anomaly inversion are not interpreted as very thin continental or oceanic crust. Sediment corrected RDA and RDA_{CT} (shown in Fig. 3f) are both negative in zone B, corresponding to the presence of crust which is thinner than 7 km or anomalous subsidence. The continental lithosphere thinning factors from gravity anomaly inversion and subsidence analysis assuming a serpentinized mantle solution are 1.0 consistent with the presence of serpentinized exhumed mantle.

The interface between zones B and C corresponds to the boundary between thinned continental crust and exhumed mantle and is located by the inflection points in Moho depth, RDAs and continental lithosphere thinning factors determined assuming a solution for serpentinized mantle. Gravity anomaly inversion, RDA and subsidence analysis results show that the OCT along IAM9 is relatively

Table 1. Summary of crustal types encountered along the western Iberian profiles and the consequent ranges of crustal basement thicknesses, continental lithosphere thinning factors and residual depth anomaly results predicted from the integrated analysis techniques.

	Crustal thickness (km)	Continental lithosphere thinning factors (from gravity inversion and subsidence analysis)			Residual depth anomaly (m) *Assuming no mantle dynamic topography effects for sediment corrected RDA	
		Assuming normal magmatic	Assuming magma starved	Assuming serpentinized mantle	*RDA_{SC}	RDA_{CT}
Oceanic crust (normal thickness)	7	1.0	0.8	0.9	Zero	Zero
Oceanic crust (thin crust to magma poor)	0 to < 7	1.0	0.8 to 1	0.9 to 1.0	Negative	Negative
Serpentinized exhumed mantle	0 to 3	1.0	0.9	1.0	Negative	Negative
Hyper-extended continental crust	5 to 10	0.7–1.0	0.7–0.85	0.7–0.95	Negative to slightly positive	Negative to slightly positive
Continental crust (within necking zone)	10 to 25	0.3–0.7	0.3–0.7	0.3–0.7	Slightly positive to very positive	Slightly positive to very positive
Continental crust (inboard of necking zone)	25+	0.0–0.3	0.0–0.3	0.0–0.3	Very positive	Very positive

narrow, with the distance between the COB and the proximal start of the necking zone measuring less than 100 km.

5.1.3 Zones C, D and E: continental crust

In zones C, D and E, the crustal basement thicknesses increase gradually to approximately 35 km at the eastern end of the profile, although the poor resolution of sediment thickness in this region may result in an overestimate of Moho depth. Both the sediment corrected RDA and RDA_{CT} (shown in Fig. 3f) increase eastwards. The continental lithosphere thinning factors from gravity anomaly inversion and subsidence analysis show a corresponding eastwards decrease. We tentatively interpret the composite analysis plot (Fig. 11) to show the location of hyper-extended continental crust and the crustal necking zone. The combined width of the hyper-extended continental crust and necking zone appears to be very narrow and it is difficult to place the transition from one to the other.

Fig. 11(e) shows a comparison of our interpretations of the crustal types along the IAM9 profile with those interpreted by Dean *et al.* (2000) and Bronner *et al.* (2011). Our interpreted location of the boundary between oceanic crust and exhumed mantle is similar to that interpreted by Dean *et al.* (2000) although we place the boundary between continental crust and exhumed mantle slightly more landward. Although the interpreted boundary between oceanic crust and exhumed mantle from Bronner *et al.* (2011) is significantly more distal than our interpreted boundary, it does correspond to slight changes in crustal basement thickness, RDAs and continental lithosphere thinning factors determined assuming magma-starved or a serpentinized mantle solution.

5.2 Lusigal 12

The composite analysis plot for the Lusigal 12 profile in the Iberian Abyssal Plain (Fig. 12) is interpreted as showing two distinct crustal types: serpentinized exhumed mantle (zone B), and thinned continental crust, which can be further subdivided into hyperextended continental crust (zone C) and the crustal necking zone (zone D). No unequivocal oceanic crust of 'normal' thickness (corresponding to zone A on the IAM9 profile) is evident on Lusigal 12. The interpretation of these zones of serpentinized exhumed mantle and thinned continental crust, and their boundary, along Lusigal 12 have been validated against ODP well data and other previous studies (e.g. Péron-Pinvidic & Manatschal 2009; Sutra & Manatschal 2012).

The discussions below refer to Fig. 12, unless otherwise stated.

5.2.1 Zone B: exhumed mantle

In zone B, the crustal basement thicknesses predicted, from gravity anomaly inversion, range between 2 and 4 km. These very low values of crustal thickness are interpreted as being indicative of serpentinized exhumed mantle (see earlier discussion for IAM9). Both the sediment corrected RDA and RDA_{CT} (Fig. 6b) are negative in this region. The sediment corrected RDA is negative between −500 and −1500 m, implying that the crust in this region is substantially less than 7 km thick or that there is anomalous subsidence. The continental lithosphere thinning factors for the serpentinized mantle solution from the gravity anomaly inversion show a value of 1.0 in this region consistent with the presence of serpentinized exhumed mantle; whilst from subsidence analysis they range between 0.95 and 1.0. Both the gravity anomaly inversion and subsidence analysis thinning factors show a marked inflection at the inner boundary of zone B. For zone B, a serpentinized mantle solution is preferred, as it predicts high thinning factors without the requirement of magmatic addition (and the formation of oceanic crust).

The COB, corresponding to the interface between zones B and C, is located by the inflection points in Moho depth, RDAs and continental lithosphere thinning factors determined for solutions assuming both magma-starved and serpentinized mantle. Gravity anomaly inversion, RDA and subsidence analysis results show that the OCT along Lusigal 12 is wider than that for IAM9, with the distance between the COB and the proximal start of the necking zone measuring more than 150 km.

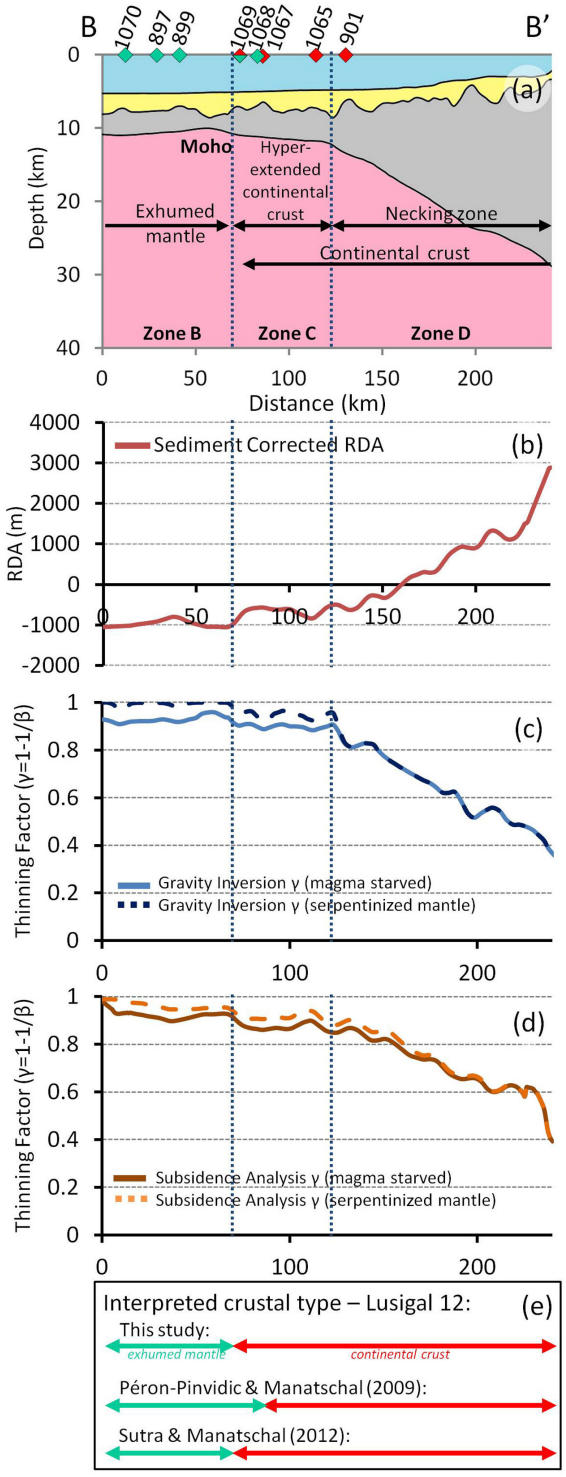

Figure 12. Composite analysis plot along Lusigal 12, showing interpretations of crustal basement types made from the integrated quantitative analysis. (a) Crustal cross section along Lusigal 12 (B–B′) from gravity anomaly inversion. ODP well locations are identified and colour coded by crustal type (see ODP well key on Fig. 5b). (b) Sediment corrected RDA along Lusigal 12. (c) Continental lithosphere thinning factors (γ) from gravity anomaly inversion assuming a magma-starved and a serpentinized mantle solution. (d) Continental lithosphere thinning factors (γ) from subsidence analysis assuming a magma-starved and a serpentinized mantle solution. Our interpreted boundaries between the crustal zones are indicated by the dashed lines. (e) Comparison of our interpreted crustal types with those from Péron-Pinvidic & Manatschal (2009) and Sutra & Manatschal (2012).

Table 2. ODP well observations along Lusigal 12 (Boillot *et al.* 1987; Sawyer *et al.* 1994; Whitmarsh & Sawyer 1996; Whitmarsh *et al.* 1998; Tucholke *et al.* 2007).

ODP well	Description
1070	Serpentinized peridotite
897	Serpentinized mantle
899	Serpentinized breccia
1069	Carbonates, upper crust
1068	Serpentinized peridotite (overlain by polymict breccias)
1067	Amphibolite, minor tonalite, meta-gabbros
1065	Pre-tectonic sediments (carbonates) over upper crust
901	Pre-tectonic sediments (carbonates) over upper crust

5.2.2 Zones C and D: continental crust

In zones C and D, crustal thicknesses predicted from gravity anomaly inversion increase eastwards towards the continent, as do the sediment corrected RDAs and RDA_{CT} (Fig. 6b), whilst the continental lithosphere thinning factors from gravity anomaly inversion and subsidence analysis decrease. This is indicative of zone C and D corresponding to thinned continental crust. A magma-starved solution for the prediction of RDA and continental lithosphere thinning factors is preferred for this zone. We identify the boundary between hyperextended crust (zone C) and the crustal necking zone (zone D) using a combination of changes in crustal basement thickness, variations in RDA and changes in continental lithosphere thinning factors.

We compare our interpretation of the crustal types along the Lusigal 12 profile with those interpreted by Péron-Pinvidic & Manatschal (2009) and Sutra & Manatschal (2012) in Fig. 12(e). Our interpretation of the boundary between oceanic crust and exhumed mantle compares well with both.

5.2.3 Comparison with ODP well observations

Observations from the ODP drill logs (897, 899, 901, 1065, 1067, 1068, 1069 and 1070) along Lusigal 12 are summarized in Fig. 12(a) and in Table 2. Our interpretation of crustal types from the composite analysis plot (Fig. 12) and summarized in Fig. 12(e) is consistent with the ODP well observations. ODP well logs (1070, 899 and 897), in zone B, show the presence of serpentinized peridotite, serpentinite, serpentinized plagioclase, breccia and mantle, which are in agreement with our interpretation of the presence of exhumed mantle from the composite analysis plot. The ODP wells (1069, 1068, 1067, 1065 and 901), in zone C, indicate the presence of pre-tectonic outer-shelf carbonates, which suggest the occurrence of upper continental crust, which is in agreement with our interpretations of the composite analysis plot.

5.3 ISE-01

Interpretation of the composite analysis plots of profile ISE-01 on Galicia Bank (Fig. 13) suggests that there are two crustal types along the profile; exhumed mantle (zone B) and continental crust, which can be subdivided into hyper-extended crust (zone C), the crustal necking zone (zone D) and proximal continental crust (zone E). These interpretations, based on gravity anomaly inversion, RDA and subsidence analysis, are consistent with ODP well data on profile ISE-01. As with Lusigal 12, no oceanic crust of 'normal' thickness (corresponding to zone A on the IAM9 profile) is evident on ISE-01.

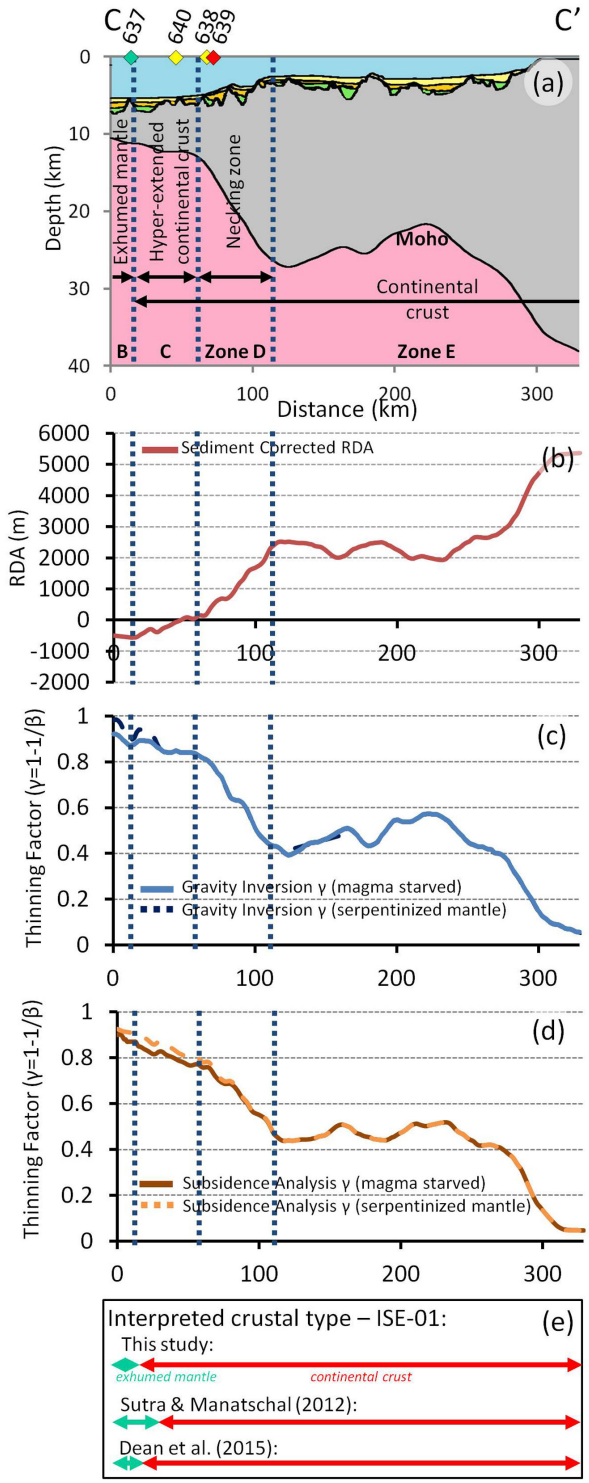

Figure 13. Composite analysis plot along the ISE-01 profile, showing interpretations of crustal basement types made from the integrated quantitative analysis. (a) Crustal cross section along the ISE-01 profile (C–C′) from gravity anomaly inversion. ODP well locations are identified and colour coded by crustal type (see ODP well key on Fig. 5b). (b) Sediment corrected RDA along the ISE-01 profile. (c) Continental lithosphere thinning factors (γ) from gravity anomaly inversion assuming a magma-starved and a serpentinized mantle solution. (d) Continental lithosphere thinning factors (γ) from subsidence analysis assuming a magma-starved and a serpentinized mantle solution. Our interpreted boundaries between the crustal zones are indicated by the dashed lines. (e) Comparison of our interpreted crustal types with those from Sutra & Manatschal (2012) and Dean *et al.* (2015).

The discussions below refer to Fig. 13, unless otherwise stated.

5.3.1 *Zone B: exhumed mantle*

In zone B at the western end of the profile, crustal basement thicknesses, from gravity anomaly inversion, range between 4 and 5 km and RDA analysis shows negative sediment corrected RDAs and RDA_{CT} (Fig. 9b) in this region. The low values of crustal thickness from gravity anomaly inversion in this region (and the resulting RDA_{CT} ranging between zero and −1000 m) are interpreted as being indicative of serpentinized exhumed mantle (see earlier discussion for IAM9). The sediment corrected RDA ranges between zero and −800 m, which implies either the presence of crust, which is thinner than 7 km, or anomalous subsidence. In zone B, if a serpentinized mantle solution is assumed, the continental lithosphere thinning factors reach 1.0 from gravity anomaly inversion and exceed 0.9 from subsidence analysis, which we interpret as indicating the start of serpentinized exhumed mantle.

The COB for profile ISE-01 is interpreted as being at the interface between zones B and C and corresponds to inflection points in Moho depth, RDA and continental lithosphere thinning factors determined assuming the serpentinized mantle solution. In contrast to profiles IAM9 and Lusigal 12, ISE-01 shows a very broad region between the proximal start of the necking zone and COB; the distance separating these is of the order 250 km.

5.3.2 *Zones C, D and E: continental crust*

In zones C, D and E, the crustal basement thickens and the RDA values increase eastwards towards the continent. These and the corresponding decrease in continental lithosphere thinning factors imply the presence of thinned continental crust in these zones. Continental lithosphere thinning factors predicted from gravity anomaly inversion are in good agreement with those predicted from subsidence analysis.

In Fig. 13(e) we compare our interpretation of the location of crustal types with those of Sutra & Manatschal (2012) and Dean *et al.* (2015). The three interpretations are in close agreement. The 'western extension 2 (WE2)' seismic reflection line of Dean *et al.* (2015) lies close and parallel to the ISE-01 profile and supports the existence of hyperextended crust within our interpreted zone C. Zelt *et al.* (2003) do not interpret their seismic cross-section in terms of crustal types.

5.3.3 *Comparison with ODP well observations*

Observations from the ODP drill logs (637, 638, 639 and 640) along profile ISE-01 are summarized in Fig. 13(a) and Table 3 and have been compared to our interpretations made from the integrated quantitative analysis shown on the composite analysis plot for profile

Table 3. ODP well observations along ISE-01 (Boillot *et al.* 1987; Sawyer *et al.* 1994; Whitmarsh & Sawyer 1996; Whitmarsh *et al.* 1998; Tucholke *et al.* 2007).

ODP Well	Description
637	Serpentinized peridotite
640	Syn-rift sediments
638	Syn-rift sediments
639	Continental basement

ISE-01. Our interpretations are consistent with the ODP well data. The ODP well 637, in zone B, shows the presence of serpentinized peridotite, whilst ODP well 639, in zone C, shows the presence of continental basement. The interpretation of the composite analysis plot for profile ISE-01 is consistent with the ODP observations at both of these wells. ODP well logs 638 and 640, in zone C, are much shallower only showing the presence of syn-rift sediments.

6 CONCLUSION

The gravity anomaly inversion, RDA and subsidence analysis techniques are of global applicability and may be used on many deep-water frontier rifted continental margins, in order to assist in understanding the large scale distribution of thinned continental crust and lithosphere, the start of unequivocal oceanic crust and hence determine the structure of the OCT, COB location and magmatic type. Testing of these techniques has been carried out on the west Iberian rifted continental margin, as this is one of the best-studied margins worldwide, due to the abundance of ODP well data. Integrated quantitative analysis of the west Iberian seismic profiles (IAM9, Lusigal 12 and ISE-01) has enabled further geological interpretations to be made of the crustal structure and distribution, which are validated using ODP well data, and where ODP well data are ambiguous, predictions have been made. Integrated quantitative analysis of the west Iberian seismic profiles show the crustal structure and the distribution of thinned continental crust, exhumed mantle and the start of unequivocal oceanic crust (where present) along the margin. The integrated approach, which considers the gravity anomaly inversion, RDA and subsidence analysis techniques together, has enabled a less subjective geological interpretation of the OCT structure along the seismic profiles and a more accurate prediction of the COB location to be made. Predicted distances between the COB and the proximal start of the necking zone for the west Iberian margin range between 100 and 250 km, with the greatest distances predicted for Galicia Bank. Our interpretation of crustal types based on our composite analysis has been compared with that of previous workers and is generally consistent.

An accurate identification of the crustal structure and the distribution of continental and oceanic crust remains crucial in order to fully understand the evolution of the west Iberian rifted continental margin, with fundamental implications for building a better geodynamic history and plate tectonic reconstruction model, and for the evolution of petroleum systems. We suggest that the integrated quantitative analysis techniques described in this paper provide useful assistance to high receiver-density wide-angle seismology and deep-long offset reflection seismology for the determination of OCT structure, COB location and crustal type at rifted continental margins.

ACKNOWLEDGEMENTS

LC was funded by the MM3 industry consortium. We thank Tim Minshull for his constructive and encouraging reviews.

REFERENCES

Alvey, A., Gaina, C., Kusznir, N.J. & Torsvik, T.H., 2008. Integrated crustal thickness mapping and plate reconstructions for the high Arctic, *Earth planet. Sci. Lett.,* **274**(3–4), 310–321.

Amante, C. & Eakins, B.W., 2009. ETOPO1 1 Arc-minute global relief model: procedures, data sources and analysis, *NOAA Technical Memorandum NESDIS NGDC-24,* p. 19.

Aslanian, D. *et al.*, 2009. Brazilian and African passive margins of the central segment of the South Atlantic Ocean: kinematic constraints, *Tectonophysics,* **468**(1–4), 98–112.

Autin, J. *et al.*, 2010. Continental break-up history of a deep magma-poor margin based on seismic reflection data (northeastern Gulf of Aden margin, offshore Oman, *Geophys. J. Int.,* **180**(2), 501–519.

Boillot, G. *et al.*, 1987. Tectonic denudation of the upper mantle along passive margins: a model based on drilling results (ODP leg 103, western Galicia margin, Spain), *Tectonophysics,* **132**(4), 335–342.

Boillot, G., Grimaud, S., Mauffret, A., Mougenot, D., Kornprobst, J., Mergoil-Daniel, J. & Torrent, G., 1980. Ocean-continent boundary off the Iberian margin: a serpentinite diapir west of the Galicia Bank, *Earth planet. Sci. Lett.,* **48**(1), 23–34.

Bronner, A., Sauter, D., Manatschal, G., Peron-Pinvidic, G. & Munschy, M., 2011. *Magmatic Breakup as An Explanation for Magnetic Anomalies At Magma-Poor Rifted Margins, Nature Geoscience,* Vol. 4, Nature Publishing Group, a division of Macmillan Publishers Limited. All Rights Reserved, 5 p.

Carlson, R.L. & Herrick, C.N., 1990. Densities and porosities in the oceanic crust and their variations with depth and age, *J. geophys. Res.: Solid Earth,* **95**(B6), 9153–9170.

Chappell, A.R. & Kusznir, N.J., 2008. Three-dimensional gravity inversion for Moho depth at rifted continental margins incorporating a lithosphere thermal gravity anomaly correction, *Geophys. J. Int.,* **174**(1), 1–13.

Chian, D., Louden, K.E., Minshull, T.A. & Whitmarsh, R.B., 1999. Deep structure of the ocean-continent transition in the southern Iberia Abyssal Plain from seismic refraction profiles: Ocean Drilling Program (Legs 149 and 173) transect, *J. geophys. Res.: Solid Earth,* **104**(B4), 7443–7462.

Christensen, N.I. & Mooney, W.D., 1995. Seismic velocity structure and composition of the continental crust: a global view, *J. geophys. Res.: Solid Earth,* **100**(B6), 9761–9788.

Coffin, M.F. & Eldholm, O., 1994. Large igneous provinces: crustal structure, dimensions, and external consequences, *Rev. Geophys.,* **32**(1), 1–36.

Cole, P.B., Minshull, T.A. & Whitmarsh, R.B., 2002. Azimuthal seismic anisotropy in a zone of exhumed continental mantle, West Iberia margin, *Geophys. J. Int.,* **151**(2), 517–533.

Contrucci, I. *et al.*, 2004. Deep structure of the West African continental margin (Congo, Zaïre, Angola), between 5°S and 8°S, from reflection/refraction seismics and gravity data, *Geophys. J. Int.,* **158**(2), 529–553.

Cooper, C., 2010. Anomalous bathymetry and mass heterogeneity at the conjugate Iberia and Newfoundland rifted margins, *PhD thesis,* University of Liverpool, 260 p.

Cowie, L. & Kusznir, N., 2012. Mapping crustal thickness and oceanic lithosphere distribution in the Eastern Mediterranean using gravity inversion, *Petrol. Geosci.,* **18**(4), 373–380.

Crosby, A.G. & McKenzie, D., 2009. An analysis of young ocean depth, gravity and global residual topography, *Geophys. J. Int.,* **178**(3), 1198–1219.

Crosby, A.G., McKenzie, D. & Sclater, J.G., 2006. The relationship between depth, age and gravity in the oceans, *Geophys. J. Int.,* **166**(2), 553–573.

D'Acremont, E., Leroy, S., Beslier, M.-O., Bellahsen, N., Fournier, M., Robin, C., Maia, M. & Gente, P., 2005. Structure and evolution of the eastern Gulf of Aden conjugate margins from seismic reflection data, *Geophys. J. Int.,* **160**(3), 869–890.

Dean, S.M., Minshull, T.A., Whitmarsh, R.B. & Louden, K.E., 2000. Deep structure of the ocean-continent transition in the southern Iberia Abyssal Plain from seismic refraction profiles: the IAM-9 transect at 40°20′N, *J. geophys. Res.: Solid Earth,* **105**(B3), 5859–5885.

Dean, S.L., Sawyer, D.S. & Morgan, J.K., 2015. Galicia Bank ocean-continent transition zone: new seismic reflection constraints, *Earth planet. Sci. Lett.,* **413,** 197–207.

Discovery 215 Working Group, Minshull, T.A., Dean, S.M., Whitmarsh, R.B., Russell, S.M., Louden, K.E. & Chian, D., 1998. Deep structure in the vicinity of the ocean-continent transition zone under the southern Iberia Abyssal Plain, *Geology,* **26**(8), 743–746.

Franke, D., 2013. Rifting, lithosphere breakup and volcanism: comparison of magma-poor and volcanic rifted margins, *Mar. Petrol. Geol.,* **43**(0), 63–87.

Greenhalgh, E.E. & Kusznir, N.J., 2007. Evidence for thin oceanic crust on the extinct Aegir Ridge, Norwegian Basin, NE Atlantic derived from satellite gravity inversion, *Geophys. Res. Lett.,* **34**(6), L06305, doi:10.1029/2007GL029440.

Henning, A.T., Sawyer, D.S. & Templeton, D.C., 2004. Exhumed upper mantle within the ocean-continent transition on the northern West Iberia margin: evidence from prestack depth migration and total tectonic subsidence analyses, *J. geophys. Res.: Solid Earth,* **109**(B5), doi:10.1029/2003JB002526.

Hinz, K., 1981. A hypothesis on terrestrial catastrophes: wedges of very thick oceanward dipping layers beneath passive continental margins—their origin and paleoenvironmental significance, *Geologisches Jahrbuch Reihe E,* **22,** 3–28.

Hopper, J.R., Funck, T., Tucholke, B.E., Larsen, H.C., Holbrook, W.S., Louden, K.E., Shillington, D. & Lau, H., 2004. Continental breakup and the onset of ultraslow seafloor spreading off Flemish Cap on the Newfoundland rifted margin, *Geology,* **32**(1), 93–96.

Jordan, T.H. & Anderson, D.L., 1974. Earth structure from free oscillations and travel times, *Geophys. J. R. astr. Soc.,* **36**(2), 411–459.

Kusznir, N. & Karner, G., 1985. Dependence of the flexural rigidity of the continental lithosphere on rheology and temperature, *Nature,* **316**(6024), 138–142.

Kusznir, N.J., Roberts, A.M. & Morley, C.K., 1995. Forward and reverse modelling of rift basin formation, *Geol. Soc., Lond., Spec. Publ.,* **80**(1), 33–56.

Manatschal, G., 2004. New models for evolution of magma-poor rifted margins based on a review of data and concepts from West Iberia and the Alps, *Int. J. Earth Sci.,* **93**(3), 432–466.

Manatschal, G., Froitzheim, N., Rubenach, M. & Turrin, B.D., 2001. The role of detachment faulting in the formation of an ocean-continent transition: insights from the Iberia Abyssal Plain, *Geol. Soc., Lond., Spec. Publ.,* **187**(1), 405–428.

Manatschal, G., Sutra, E. & Péron-Pinvidic, G., 2010. The lesson from the Iberia-Newfoundland rifted margins: how applicable is it to other rifted margins?, in *Proceedings 2nd Central & North Atlantic Conjugate Margins,* Rediscovering the Atlantic, New Insights, New winds for an old sea, Vol. 2, pp. 27–37.

McKenzie, D., 1978. Some Remarks on the Development of Sedimentary Basins, *Earth planet. Sci. Lett.,* **40,** 25–32.

Müller, R.D., Roest, W.R., Royer, J.-Y., Gahagan, L.M. & Sclater, J.G., 1997. Digital isochrons of the world's ocean floor, *J. geophys. Res.,* **102**(B2), 3211–3214.

Müller, R.D., Sdrolias, M., Gaina, C., Steinberger, B. & Heine, C., 2008. Long-term sea-level fluctuations driven by ocean basin dynamics, *Science,* **319**(5868), 1357–1362.

Parker, R.L., 1972. The rapid calculation of potential anomalies, *Geophys. J. R. astr. Soc.,* **31**(4), 447–455.

Parsons, B. & Sclater, J.G., 1977. An analysis of the variation of ocean floor bathymetry and heat flow with age, *J. geophys. Res.,* **82**(5), 803–827.

Pérez-Gussinyé, M., 2012. A tectonic model for hyperextension at magma-poor rifted margins: an example from the West Iberia–Newfoundland conjugate margins, *Geol. Soc., Lond., Spec. Publ.* No. 369, doi:10.1144/SP369.19.

Péron-Pinvidic, G. & Manatschal, G., 2009. The final rifting evolution at deep magma-poor passive margins from Iberia-Newfoundland: a new point of view, *Int. J. Earth Sci.*, **98**(7), 1581–1597.

Péron-Pinvidic, G., Manatschal, G., Minshull, T.A. & Sawyer, D.S., 2007. Tectonosedimentary evolution of the deep Iberia-Newfoundland margins: evidence for a complex breakup history, *Tectonics,* **26**(2), TC2011, doi:10.1029/2006TC001970.

Pickup, S.L.B., Whitmarsh, R.B., Fowler, C.M.R. & Reston, T.J., 1996. Insight into the nature of the ocean-continent transition off West Iberia from a deep multichannel seismic reflection profile, *Geology,* **24**(12), 1079–1082.

Reston, T.J., 2009. The structure, evolution and symmetry of the magma-poor rifted margins of the North and Central Atlantic: a synthesis, *Tectonophysics,* **468**(1–4), 6–27.

Roberts, A.M., Kusznir, N.J., Yielding, G. & Styles, P., 1998. 2D flexural backstripping of extensional basins; the need for a sideways glance, *Petrol. Geosci.,* **4**(4), 327–338.

Roberts, A.M., Kusznir, N.J., Corfield, R.I., Thompson, M. & Woodfine, R., 2013. Integrated tectonic basin modelling as an aid to understanding deep-water rifted continental margin structure and location, *Petrol. Geosci.,* **19**(1), 65–88.

Russell, S.M. & Whitmarsh, R.B., 2003. Magmatism at the west Iberia non-volcanic rifted continental margin: evidence from analyses of magnetic anomalies, *Geophys. J. Int.,* **154**(3), 706–730.

Sandwell, D.T. & Smith, W.H.F., 2009. Global marine gravity from retracked Geosat and ERS-1 altimetry: ridge segmentation versus spreading rate, *J. geophys. Res.,* **114**(B1), B01411, doi:10.1029/2008JB006008.

Sawyer, D.S., Whitmarsh, R.B. & Klaus, A., 1994. Proceedings of the ODP, Initial Reports, 149, College Station, TX (Ocean Drilling Program).

Sclater, J.G. & Christie, P.A.F., 1980. Continental stretching: an explanation of the Post-Mid-Cretaceous subsidence of the central North Sea Basin, *J. geophys. Res.: Solid Earth,* **85**(B7), 3711–3739.

Skelton, A., Whitmarsh, R., Arghe, F., Crill, P. & Koyi, H., 2005. Constraining the rate and extent of mantle serpentinization from seismic and petrological data: implications for chemosynthesis and tectonic processes, *Geofluids,* **5**(3), 153–164.

Stein, C.A. & Stein, S., 1992. A model for the global variation in oceanic depth and heat flow with lithospheric age, *Nature,* **359**(6391), 123–129.

Sutra, E. & Manatschal, G., 2012. How does the continental crust thin in a hyperextended rifted margin? Insights from the Iberia margin, *Geology,* **40**(2), 139–142.

Sutra, E., Manatschal, G., Mohn, G. & Unternehr, P., 2013. Quantification and restoration of extensional deformation along the Western Iberia and Newfoundland rifted margins, *Geochem. Geophys. Geosyst.,* **14**(8), 2575–2597.

Tucholke, B.E. & Ludwig, W.J., 1982. Structure and origin of the J Anomaly Ridge, western North Atlantic Ocean, *J. geophys. Res.: Solid Earth,* **87**(B11), 9389–9407.

Tucholke, B.E., Sawyer, D.S. & Sibuet, J.C., 2007. Breakup of the Newfoundland–Iberia rift, *Geol. Soc., Lond., Spec. Publ.,* **282**(1), 9–46.

Unternehr, P., Péron-Pinvidic, G., Manatschal, G. & Sutra, E., 2010. Hyper-extended crust in the South Atlantic: in search of a model, *Petrol. Geosci.,* **16**(3), 207–215.

White, R. & McKenzie, D., 1989. Magmatism at rift zones: the generation of volcanic continental margins and flood basalts, *J. geophys. Res.*, **94**(B6), 7685–7729.

White, R.S., McKenzie, D. & O'Nions, R.K., 1992. Oceanic crustal thickness from seismic measurements and rare earth element inversions, *J. geophys. Res.,* **97**(B13), 19 683–19 715.

White, R.S., Smith, L.K., Roberts, A.W., Christie, P.A.F. & Kusznir, N.J., 2008. Lower-crustal intrusion on the North Atlantic continental margin, *Nature,* **452**(7186), 460–464.

Whitmarsh, R.B. & Miles, P.R., 1995. Models of the development of the West Iberia rifted continental margin at 40°30′N deduced from surface and deep-tow magnetic anomalies, *J. geophys. Res.: Solid Earth,* **100**(B3), 3789–3806.

Whitmarsh, R.B. & Sawyer, D.S., 1996. The ocean-continent transition beneath the Iberia Abyssal Plain and continental rifting to seafloor spreading processes, in *Proceedings of the Ocean Drilling Program, Scientific Results 149,* pp. 713–733, eds Whitmarsh, R.B., Sawyer, D.S., Klaus, A. & Masson, D.G., College Station, TX.

Whitmarsh, R.B., Beslier, M.O. & Wallace, P.J., 1998. Proceedings of the ODP, Initial Reports, 173, College Station, TX (Ocean Drilling Program).

Whitmarsh, R.B., Minshull, T.A., Russell, S.M., Dean, S.M., Louden, K.E. & Chian, D., 2001. The role of syn-rift magmatism in the rift-to-drift evolution of the West Iberia continental margin: geophysical observations, *Geol. Soc., Lond., Spec. Publ.,* **187**(1), 107–124.

Wilson, J.T., 1966. Did the Atlantic close and then re-open?, *Nature,* **211**(5050), 676–681.

Zalán, P.V., Severino, M.C.G., Rigoti, C., Magnavita, L.P., Oliveira, J.A.B. & Viana, A.R., 2011. An entirely new 3D-view of the crustal and mantle structure of a ruptured South Atlantic passive margin—Santos, Campos and Espírito Santo Basins, Brazil (Expanded Abstract), *in Proceedings of the AAPG Annual Convention & Exhibition Abstracts Volume CDROM,* Paper 986156.

Zelt, C.A., Sain, K., Naumenko, J.V. & Sawyer, D.S., 2003. Assessment of crustal velocity models using seismic refraction and reflection tomography, *Geophys. J. Int.,* **153**(3), 609–626.

APPENDIX: THE MASS DEFICIENCY OF SERPENTINIZED EXHUMED MANTLE

Seismic refraction data on the exhumed serpentinized mantle of the IAM9 seismic profile have been interpreted by Cole *et al.* (2002) and Skelton *et al.* (2005) to determine the variation in the degree of serpentinization with depth. Their results (Fig. A1a) summarized by Cooper (2010) suggest that serpentinization approaches 100 per cent in the top 1.5–2.0 km below top basement, but then attenuates with depth reaching approximately 5 per cent serpentinization at 5 km depth. Cooper (2010), following the scheme of Skelton *et al.* (2005), determined the variation of density with depth (Fig. A1b) for the serpentinized mantle of IAM9 as a function of magnetite content; his preferred density-depth model uses 4.5 per cent magnetite.

The integrated mass-deficiency of serpentinized mantle with respect to un-serpentinized mantle assuming 4.5 per cent magnetite content is shown in Fig. A1(c) as a function of depth. The plot shows that the majority of the mass deficiency of serpentinized mantle derives from the topmost 2–3 km of serpentinized mantle, and that the mass deficiency reaches a constant asymptotic maximum (the degree of serpentinization tends to zero as depth increases). For comparison the mass deficiency of crustal basement with a density of 2850 kg m^{-3} with respect to mantle (assumed density = 3300 kg m^{-3}) is shown as a function of the depth to the base of crustal basement (i.e. crustal basement thickness). The plot shows that the mass deficiency of serpentinized exhumed mantle is equivalent to the mass deficiency of crustal basement with a thickness of 3.1 km.

The density of serpentinized mantle is important for both the determination of Moho depth from gravity anomaly inversion, and also for subsidence analysis to determine lithosphere stretching and thinning factors. The analysis based on IAM9 summarized above suggests that the gravitational and isostatic signals of serpentinized exhumed mantle are equivalent to a crustal basement thickness of approximately 3 km.

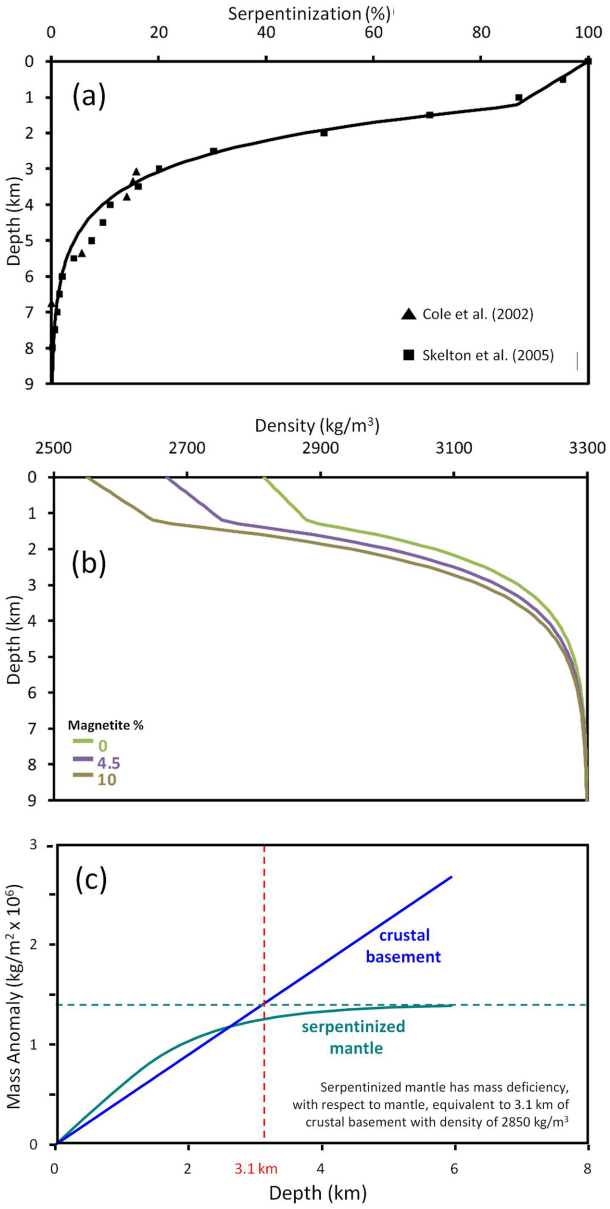

Figure A1. (a) The degree of serpentinization as a function of depth for serpentinized exhumed mantle on seismic line IAM9 determined by Cole *et al.* (2002) and Skelton *et al.* (2005) and summarized by Cooper (2010). (b) Density as a function of depth for serpentinized exhumed mantle for line IAM9 determined by Cooper (2010) and showing sensitivity to magnetite content. (c) Mass deficiency of serpentinized mantle with respect to unaltered mantle as a function of serpentinization depth compared with the mass deficiency of crustal basement with density 2850 kg m^{-3}. Serpentinized exhumed mantle has a mass deficiency with respect to unaltered mantle equivalent to crustal basement which is approximately 3 km thick.